MEASUREMENT OF THE PROPAGATION CHARACTERISTICS OF

SHIELDED AND UNSHIELDED DIELECTRIC-TUBE WAVEGUIDES

by

IKUFUMI MAKINO

B.Sc., Doshisha University, 1967

A THESIS SUBMITTED IN PARTIAL FULFILMENT OF THE

REQUIREMENTS FOR THE DEGREE OF

MASTER OF APPLIED SCIENCE

in the Department of

Electrical Engineering

We accept this thesis as conforming to the

required standard

Research Supervisors...

....

Members of the Committee ....

....

Head of Department ....

Members of the Department of

Electrical Engineering

THE UNIVERSITY OF BRITISH COLUMBIA

December, 1970

Department of Electrical Engineering

The University of British Columbia
Vancouver 8, Canada

Date December 11, 1970

ABSTRACT

Accurate measurements of the propagation coefficient of the HE_{11} mode on polythene-tube waveguides in air and surrounded by a polyfoam shield are reported. These were carried out at X-band frequencies using a cavity-resonance method. The results obtained confirm previous theoretical predictions although there is an element of uncertainty concerning the exact dielectric properties of the commercial grade polythene tubes used. The measurements also yielded the phase coefficient of the HE_{11} mode which was confirmed by measurement of the radial decay of the electric field outside the tube.

Enclosing the dielectric-tube in a low-density, low-loss poly-foam shield resulted in only a slight degradation of the attenuation characteristics of the waveguides.

Measurements of the phase characteristics of the higher order TE_{01} and TM_{01} modes on the tube at frequencies close to cutoff are also reported.

TABLE OF CONTENTS

LIST OF ILLUSTRATIONS

Figure | Page

LIST OF TABLES

LIST OF SYMBOLS

a_i, b_i	= constants
$A_n(p_{ij})$, $B_n(p_{ij})$	= functions of Bessel functions
c_i	= jb_i/a_i
E_{zi}, E_{ri}, $E_{\theta i}$	= longitudinal, radial, azimuthal components of electric field, respectively, in medium i
f	= frequency
f_r	= resonant frequency
h_i	= wave number of medium i
H_{zi}, H_{ri}, $H_{\theta i}$	= longitudinal, radial, azimuthal components of magnetic field, respectively, in medium i
$I_n(p_{ij})$	= modified Bessel function of the first kind
$J_n(p_{ij})$	= Bessel function of the first kind
k_0	= phase coefficient of free space
$K_n(p_{ij})$	= modified Bessel function of the second kind
ℓ	= number of half wavelengths in resonator
L	= length of resonator
m, n	= mode subscripts
N, N_i	= total power loss per unit length and power loss per unit length in medium i, respectively
N_g	= power flow
N_p, N_{pi}	= total power loss in each end plate and power loss in each plate in medium i, respectively
p_{ij}	= $h_i r_j$
Q	= quality factor
Q_ℓ	= loaded Q factor
Q_u	= unloaded Q factor
r	= radial co-ordinate
r_1, r_2	= inner and outer radius of tube respectively

R	= normalized resistive component
R_m	= resistive component of wave impedance of a metal
S_A, S_B, S_{AB}, T_A	= integrals of functions of Bessel functions
S_I, S_K, T_I, T_K	= integrals of functions of modified Bessel functions
$\tan\delta_i$	= loss tangent of medium i
v_0 , v_g, v_p	= speed of light in free space, group velocity and phase velocity, respectively
W, W_i	= total energy storage per unit length and total energy storage per unit length in medium i, respectively
$Y_n(p_{ij})$	= Bessel function of the second kind
z	= longitudinal co-ordinate
Z_0	= impedance of free space
α	= attenuation coefficient of tube
β	= phase coefficient of tube
β_i	= coupling coefficient
Δf	= bandwidth
ε_{ri}	= relative permittivity of medium i
θ	= azimuthal co-ordinate
λ	= free space wavelength
λ_c, λ_g, λ_r	= cutoff, guide and resonant wavelength, respectively
μ_{ri}	= relative premeability of medium i
ρ	= r_1/r_2
ω	= angular frequency

ACKNOWLEDGEMENT

The author is deeply indebted to his research supervisors Dr. B. Chambers and Dr. M.M.Z. Kharadly for their encouragement and guidance throughout the course of this project.

Grateful acknowledgement is made to the National Research Council of Canada for support under grants A3344 and A7243 and to the University of British Columbia for the award of a University of British Columbia Graduate Fellowship during the academic years 1968-1970.

The author is also grateful to Mr. C.G. Chubb, Mr. D.G. Daines and Mr. J.H. Stuber for building the precision equipment and to Mr. H.H. Black for the photographic work.

The author also wishes to thank Miss Linda Morris for typing the manuscript and Mr. B. Wilbee, Mr. F. Scholz and Mr. S. Graf for their careful proofreading of the final draft.

1. INTRODUCTION

During the last forty years or so, many investigators have considered the problem of surface-wave propagation along dielectric tubes. In 1932, Zachoval[1] obtained the characteristic equation for TM_{0m} modes and solved this graphically for a range of tube parameters. Two years later, the existence of these modes was verified by Liska[2], whose measurements of guide wavelength showed good agreement with Zachoval's theory. In 1949, Astrahan[3] obtained the characteristic equations for TE_{0m} and hybrid modes and measured values of guide wavelength for the HE_{11}, TM_{01} and TE_{01} modes which agreed very well with theory. At about the same time, Jakes[4] gave expressions for the attenuation coefficients of TM_{0m} and TE_{0m} modes and measured the attenuation of the TM_{01} and TE_{01} modes on polystyrene tubes. A technique for obtaining the attenuation coefficient of any mode was outlined by Unger[5] in 1954 using a method similar to Jakes', but the analysis was completed only for the HE_{11} mode on tubes with small diameter to wavelength ratios. Mallach[6] made a rough estimate of the attenuation of the HE_{11} mode by measuring the radius at which the magnitude of the electric field fell to 1/e of its value at the tube surface. In 1968 Kharadly and Lewis[7] completed a comprehensive study of the possible usefulness of the dielectric tube as a low-loss waveguide. They concluded that a moderately thin-walled tube propagating the dominant HE_{11} mode could have propagation characteristics greatly superior to those of conventional metallic waveguides at millimeter-wave frequencies. Also, they proposed a method for overcoming the problems of supporting the tube and the degradation of performance due to adverse weather conditions or nearby obstacles. This consisted of embedding the tube in a layer of low-density, low-loss dielectric of sufficient radial extent that a negligible portion of the wave was carried outside this dielectric.

So far as is known, no accurate measurements of the attenuation characteristics of the dominant HE_{11} mode on dielectric-tubes have been made. This seems surprising in view of the fact that this mode is the one most likely to be used in practice.

The objectives of the investigation reported here were therefore:

(i) to obtain experimental data on the attenuation and phase coefficients of the HE_{11} mode on commercially available polythene tubes from direct measurements, using the cavity-resonance method.

(ii) to ascertain experimentally the effect of shielding the tube with low-density, low-loss polyfoam.

Chapter 2 reviews briefly some of the features of surface-wave propagation on dielectric-tube waveguides. The theory in this chapter is drawn from reference 7. In Chapter 3, the theory underlying the cavity-resonance method for measuring the attenuation coefficient of low-loss waveguides is discussed. This is followed in Chapter 4 by a description of the experimental apparatus used. Experimental results for the propagation characteristics of the HE_{11} mode on polythene tubes in air and surrounded by a polyfoam shield are given in Chapter 5, together with results for the phase coefficient of the TE_{01} and TM_{01} modes at frequencies close to cutoff. Conclusions drawn from this investigation and suggestions for further work are contained in Chapter 6.

2. SURFACE-WAVE PROPAGATION ON DIELECTRIC TUBE WAVEGUIDES

2.1 Field Components

The tube configuration of interest is shown in figure 2.1. It consists of two coaxial dielectric regions of infinite length and relative permittivities ε_{r1} and ε_{r2} embedded in a third infinite dielectric of relative permittivity ε_{r3}, where

$$\left.\begin{array}{ll} & \varepsilon_{r2} > \varepsilon_{r1} \\ \text{and} & \varepsilon_{r2} > \varepsilon_{r3} \end{array}\right] \quad \ldots\ldots 2.1$$

In all cases, it will be assumed that the relative permeability of the i^{th} region, μ_{ri}, is unity. Propagation is assumed in the z-direction, with t-θ-z dependence of the form $\exp j(\omega t - n\theta - \beta z)$ in the lossless case.

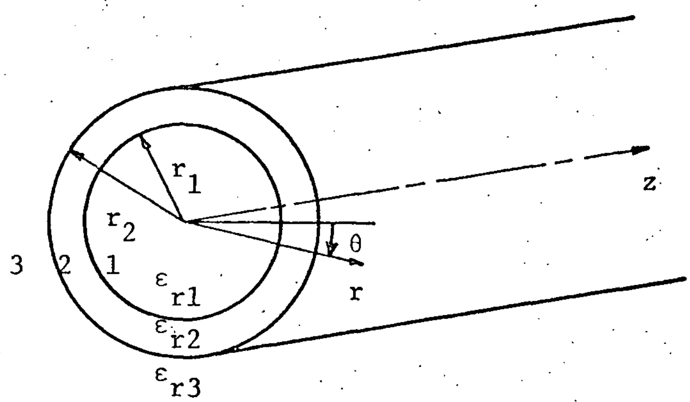

Figure 2.1 The Dielectric-Tube Waveguide

Under these conditions, omitting the factor $\exp j(\omega t - n\theta - \beta z)$, the field components are given by

$$\left.\begin{aligned}
E_{z1} &= a_1\, I_n(h_1 r) \\
E_{r1} &= j\,\frac{\beta}{h_1}\, a_1\, I_n'(h_1 r) + \frac{n\mu_{r1}\, k_0 Z_0}{h_1^2 r}\, b_1\, I_n(h_1 r) \\
E_{\theta 1} &= \frac{n\beta}{h_1^2 r}\, a_1\, I_n(h_1 r) - j\,\frac{\mu_{r1} k_0 Z_0}{h_1}\, b_1\, I_n'(h_1 r) \\
H_{z1} &= b_1\, I_n(h_1 r) \\
H_{r1} &= -\frac{n\,\varepsilon_{r1}\, k_0}{h_1^2\, r\, Z_0}\, a_1\, I_n(h_1 r) + j\,\frac{\beta}{h_1}\, b_1\, I_n'(h_1 r) \\
H_{\theta 1} &= j\,\frac{\varepsilon_{r1} k_0}{h_1 Z_0}\, a_1\, I_n'(h_1 r) + \frac{n\beta}{h_1^2\, r}\, b_1\, I_n(h_1 r)
\end{aligned}\right] \qquad 0 \le r \le r_1 \qquad \ldots\ldots\ldots\ldots\ldots 2.2.a$$

$$\left.\begin{aligned}
E_{z2} &= a_2\left[J_n(h_2 r) + \frac{a_4}{a_2}\, Y_n(h_2 r)\right] \triangleq a_2\, A_n(h_2 r) \\
E_{r2} &= -j\,\frac{\beta}{h_2}\, a_2\, A_n'(h_2 r) - \frac{n\mu_{r2}\, k_0 Z_0}{h_2^2\, r}\, b_2\, B_n(h_2 r) \\
E_{\theta 2} &= -\frac{n\beta}{h_2^2\, r}\, a_2\, A_n(h_2 r) + j\,\frac{\mu_{r2}\, k_0 Z_0}{h_2}\, b_2\, B_n'(h_2 r) \\
H_{z2} &= b_2\left[J_n(h_2 r) + \frac{b_4}{b_2}\, Y_n(h_2 r)\right] \triangleq b_2\, B_n(h_2 r) \\
H_{r2} &= \frac{n\,\varepsilon_{r2}\, k_0}{h_2^2\, r\, Z_0}\, a_2\, A_n(h_2 r) - j\,\frac{\beta}{h_2}\, b_2\, B_n'(h_2 r) \\
H_{\theta 2} &= -j\,\frac{\varepsilon_{r2}\, k_0}{Z_0\, h_2}\, a_2\, A_n'(h_2 r) - \frac{n\beta}{h_2^2\, r}\, b_2\, B_n(h_2 r)
\end{aligned}\right] \qquad r_1 \le r \le r_2 \qquad \ldots\ldots\ldots\ldots\ldots 2.2.b$$

$$\left.\begin{aligned}
E_{z3} &= a_3\, K_n(h_3 r) \\
E_{r3} &= j\,\frac{\beta}{h_3}\, a_3\, K_n'(h_3 r) + \frac{n\,\mu_{r3}\, k_0 Z_0}{h_3^2\, r}\, b_3\, K_n(h_3 r) \\
E_{\theta 3} &= \frac{n\beta}{h_3^2\, r}\, a_3\, K_n(h_3 r) - j\,\frac{\mu_{r3}\, K_0 Z_0}{h_3}\, b_3\, K_n'(h_3 r) \\
H_{z3} &= b_3 K_n(h_3 r) \\
H_{r3} &= -\frac{n\,\varepsilon_{r3}\, k_0}{h_3^2\, r\, Z_0}\, a_3\, K_n(h_3 r) + j\,\frac{\beta}{h_3}\, b_3\, K_n'(h_3 r) \\
H_{\theta 3} &= j\,\frac{\varepsilon_{r2}\, k_0}{h_3\, Z_0}\, a_3\, K_n'(h_3 r) + \frac{n\beta}{h_3^2\, r}\, b_3\, K_n(h_3 r)
\end{aligned}\right] \quad r_2 \le r \le \infty \quad \ldots\ldots\ldots\ldots 2.2.c$$

where, from the wave equation

$$\left.\begin{aligned}
h_1^2 &= \beta^2 - \mu_{r1}\, \varepsilon_{r1}\, k_0^2 \\
h_2^2 &= \mu_{r2}\, \varepsilon_{r2}\, k_0^2 - \beta^2 \\
h_3^2 &= \beta^2 - \mu_{r3}\, \varepsilon_{r3}\, k_0^2
\end{aligned}\right] \quad \ldots\ldots\ldots\ldots 2.3$$

The symbols appearing in equations 2.2 and 2.3 are defined in the list of symbols.

Upon setting n=0 (no θ-variation), equations 2.2 separate into two sets corresponding to the circularly symmetric modes designated TM_{0m} and TE_{0m}. For $n \neq 0$, equations 2.2 describe inseparable combinations of TE and TM modes which are designated hybrid modes. In general, one or other of the component parts of a hybrid mode is dominant. If the TE portion is dominant, the mode is designated HE_{nm}; if the TM component is dominant, it is termed EH_{nm}. The nature of TE or TM dominance and the significance of the subscript m in the mode designation is discussed fully in reference 7.

2.2 Mode Spectrum

2.2.1 Characteristic Equations

By matching the axial and tangential field components in media 1 and 2 at $r=r_1$ and those in media 2 and 3 at $r=r_2$, eight homogeneous equations in eight unknowns, a_i, b_i, i=1-4, are obtained. These may be solved to give the following characteristic equations for the hybrid modes:

$$\left(\frac{\varepsilon_{r2}A_n'(p_{22})}{p_{22}A_n(p_{22})}+\frac{\varepsilon_{r3}K_n'(p_{32})}{p_{32}K_n(p_{32})}\right)\left(\frac{\mu_{r2}B_n'(p_{22})}{p_{22}B_n(p_{22})}+\frac{\mu_{r3}K_n'(p_{32})}{p_{32}K_n(p_{32})}\right)=\left[\frac{n\beta}{k_0}\left(\frac{1}{p_{22}^2}+\frac{1}{p_{32}^2}\right)\right]^2 \quad \ldots\ldots\ldots 2.4.a$$

and

$$\left(\frac{\varepsilon_{r2}A_n'(p_{21})}{p_{21}A_n(p_{21})}+\frac{\varepsilon_{r1}I_n'(p_{11})}{p_{11}I_n(p_{11})}\right)\left(\frac{\mu_{r2}B_n'(p_{21})}{p_{21}B_n(p_{21})}+\frac{\mu_{r1}I_n'(p_{11})}{p_{11}I_n(p_{11})}\right)=\left[\frac{n\beta}{k_0}\left(\frac{1}{p_{11}^2}+\frac{1}{p_{21}^2}\right)\right]^2 \quad \ldots\ldots 2.4.b$$

Equation 2.4.a is applicable for EH_{nm} modes and equation 2.4.b is applicable for HE_{nm} modes. The ratio a_4/a_2 is given by equation 2.5. The ratio b_4/b_2 is obtained from equation 2.5 by interchanging ε_{ri} and μ_{ri}. The characteristic equations for the TE_{0m} and TM_{0m} modes are obtained by setting n=0 in equation 2.4.b.

A typical spectrum of modes on a polythene tube in free space ($\varepsilon_{r1}=\varepsilon_{r3}=\mu_{r1}=\mu_{r2}=\mu_{r3}=1$, $\varepsilon_{r2}=2.26$, and $\rho\overset{\Delta}{=}r_1/r_2=0.5$) is shown in figure 2.2. The main features of the mode spectrum are:

(i) The HE_{11} mode has no lower cutoff frequency.

(ii) Unlike the case for the dielectric rod ($\rho=0$), the TE_{0m} and TM_{0m} modes do not have the same value of r_2/λ at cutoff. This is also true for $HE_{1,m+1}$ and EH_{1m} modes.

(iii) As $\rho\to 1$, the phase characteristics of the TE_{0m} and HE_{1m} mode become indistinguishable, as do those of the TM_{0m} and EH_{1m} modes, thus

$$\begin{aligned}
\frac{a_4}{a_2} = -\left(\frac{J_n(p_{21})}{Y_n(p_{21})}\right) \Bigg\{ & \left(\frac{Y_n(p_{22})}{Y_n(p_{21})} - \frac{J_n(p_{22})}{J_n(p_{21})}\right) \Bigg[\left(\frac{I_n'(p_{11})}{p_{11}I_n(p_{11})}\right)\left(\frac{\varepsilon_{r1}I_n'(p_{11})}{p_{11}I_n(p_{11})} + \frac{\varepsilon_{r2}J_n'(p_{21})}{p_{21}J_n(p_{21})}\right) - \left(\frac{n^2\beta^2}{\mu_{r1}k_0^2}\right)\left(\frac{1}{p_{11}^2} + \frac{1}{p_{21}^2}\right)^2 \Bigg] \\
& + \frac{\mu_{r2}}{\mu_{r1}} \Bigg[\left(\frac{J_n'(p_{21})Y_n(p_{22})}{p_{21}J_n(p_{21})Y_n(p_{21})} - \frac{Y_n'(p_{21})J_n(p_{22})}{p_{21}Y_n(p_{21})J_n(p_{21})}\right)\left(\frac{\varepsilon_{r1}I_n'(p_{11})}{p_{11}I_n(p_{11})} + \frac{\varepsilon_{r2}J_n'(p_{21})}{p_{21}J_n(p_{21})}\right) \\
& + \frac{\left(\frac{1}{p_{11}^2} + \frac{1}{p_{21}^2}\right) J_n(p_{22})}{\left(\frac{1}{p_{22}^2} + \frac{1}{p_{32}^2}\right) J_n(p_{21})} \left(\frac{Y_n'(p_{21})}{p_{21}Y_n(p_{21})} - \frac{J_n'(p_{21})}{p_{21}J_n(p_{21})}\right)\left(\frac{\varepsilon_{r2}J_n'(p_{22})}{p_{22}J_n(p_{22})} + \frac{\varepsilon_{r3}K_n'(p_{32})}{p_{32}K_n(p_{32})}\right)\Bigg]\Bigg\} \\
\div \Bigg\{ & \left(\frac{Y_n(p_{22})}{Y_n(p_{21})} - \frac{J_n(p_{22})}{J_n(p_{21})}\right) \Bigg[\left(\frac{I_n'(p_{11})}{p_{11}I_n(p_{11})}\right)\left(\frac{\varepsilon_{r1}I_n'(p_{11})}{p_{11}I_n(p_{11})} + \frac{\varepsilon_{r2}Y_n'(p_{21})}{p_{21}Y_n(p_{21})}\right) - \left(\frac{n^2\beta^2}{\mu_{r1}k_0^2}\right)\left(\frac{1}{p_{11}^2} + \frac{1}{p_{21}^2}\right)^2 \Bigg] \\
& + \frac{\mu_{r2}}{\mu_{r1}} \Bigg[\left(\frac{J_n'(p_{21})Y_n(p_{22})}{p_{21}J_n(p_{21})Y_n(p_{21})} - \frac{Y_n'(p_{21})J_n(p_{22})}{p_{21}Y_n(p_{21})J_n(p_{21})}\right)\left(\frac{\varepsilon_{r1}I_n'(p_{11})}{p_{11}I_n(p_{11})} + \frac{\varepsilon_{r2}Y_n'(p_{21})}{p_{21}Y_n(p_{21})}\right) \\
& + \frac{\left(\frac{1}{p_{11}^2} + \frac{1}{p_{21}^2}\right) Y_n(p_{22})}{\left(\frac{1}{p_{22}^2} + \frac{1}{p_{32}^2}\right) Y_n(p_{21})} \left(\frac{Y_n'(p_{21})}{p_{21}Y_n(p_{21})} - \frac{J_n'(p_{21})}{p_{21}J_n(p_{21})}\right)\left(\frac{\varepsilon_{r2}Y_n'(p_{22})}{p_{22}Y_n(p_{22})} + \frac{\varepsilon_{r3}K_n'(p_{32})}{p_{32}K_n(p_{32})}\right)\Bigg]\Bigg\} \qquad \ldots\ldots\ldots 2.5
\end{aligned}$$

providing the physical distinction between HE and EH modes.

(iv) As $\rho \to 1$, the n=0 and n=1 modes appear in widely separated clusters, each cluster consisting of four modes (HE_{1m}, TE_{0m}, TM_{0m} and EH_{1m}).

(v) The HE_{1m} and TE_{0m} phase characteristics intersect at some value of r_2/λ. In most cases, for values of r_2/λ greater than that at the intersection, the differences in the two curves are too small to be seen graphically. However, the degeneracy of the HE_{12} and TE_{02} modes for ρ=0.5 can be seen in figure 2.2.

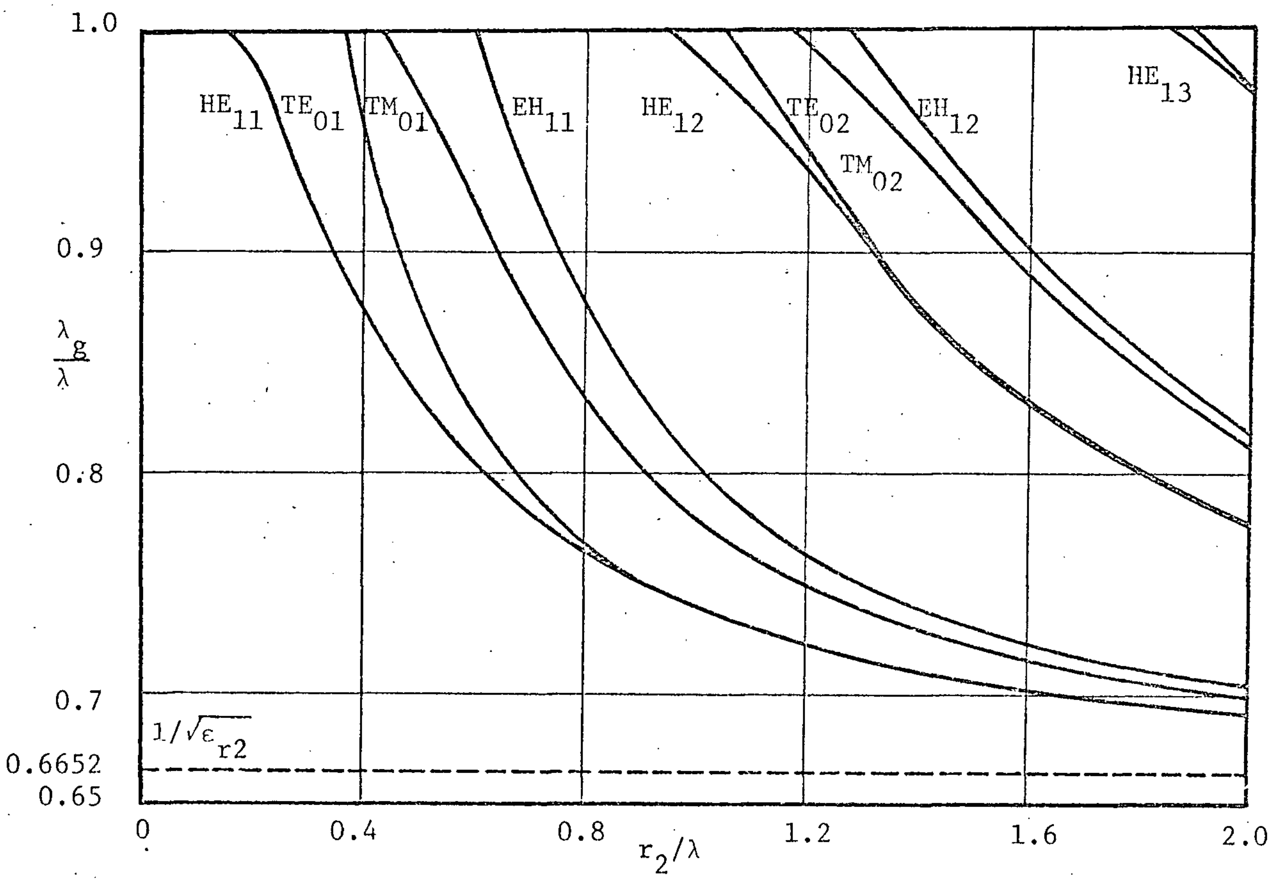

Figure 2.2 Mode Spectrum of Polythene Tube, ρ=0.5

2.2.2 Cutoff Conditions

Lossless surface-wave propagation on the dielectric-tube requires that all quantities appearing in equations 2.3 be real and positive. If $\mu_{r3}\varepsilon_{r3}=\mu_{r1}\varepsilon_{r1}$, then cutoff occurs when $h_3=0$ and $h_1=0$, or generally, when $p_{32}=0$ and $p_{11}=0$. Hence by applying small argument approximations to certain of the Bessel functions in equations 2.4.a-b, the following cutoff conditions are obtained.

$$\frac{J_0(p_{22})}{Y_0(p_{22})} = \left[\begin{array}{ll} \dfrac{\varepsilon_{r1}\, p_{21}\, J_0(p_{21}) - 2\varepsilon_{r2}\, J_1(p_{21})}{\varepsilon_{r1}\, p_{21}\, Y_0(p_{21}) - 2\varepsilon_{r2}\, Y_1(p_{21})} & \text{TM modes} \\[3em] \dfrac{p_{21}\, J_0(p_{21}) - 2J_1(p_{21})}{p_{21}\, Y_0(p_{21}) - 2Y_1(p_{21})} & \text{TE modes} \end{array}\right] \quad \ldots\ldots\ldots\ldots\ldots 2.6.a$$

$$\left.\begin{array}{ll} p_{22} = 0 & \text{HE}_{11} \text{ mode} \\[1em] \dfrac{J_1(p_{22})}{Y_1(p_{22})} = \dfrac{J_1(p_{21})}{Y_1(p_{21})} & \text{HE}_{1m} \text{ modes}, \; m > 1 \end{array}\right] \quad \ldots\ldots\ldots\ldots 2.6.b$$

$$\left[\frac{J_1'(p_{21})}{J_1(p_{22})} - \frac{Y_1'(p_{21})}{Y_1(p_{22})}\right] = \left[\frac{J_1(p_{21})}{J_1(p_{22})} - \frac{Y_1(p_{21})}{Y_1(p_{22})}\right]\left[\frac{1}{p_{21}} - \frac{p_{21}\,\varepsilon_{r1}}{(\varepsilon_{r1}+\varepsilon_{r2})}\right] \quad \text{EH}_{1m} \text{ modes}, \; m \geq 1 \quad \ldots 2.6.c$$

At cutoff p_{22} is given by

$$p_{22}=2\pi\left(\frac{r_2}{\lambda_c}\right)\sqrt{(\mu_{r2}\varepsilon_{r2} - \mu_{r3}\varepsilon_{r3})} \quad \ldots\ldots\ldots\ldots\ldots\ldots\ldots\ldots 2.7$$

from which the value of r_2/λ_c can be determined.

The variation of r_2/λ_c with ρ for the TE_{01}, TM_{01}, EH_{11} and HE_{12} modes on a polythene tube (ε_{r2}=2.26) in free space is shown in figure 2.3.

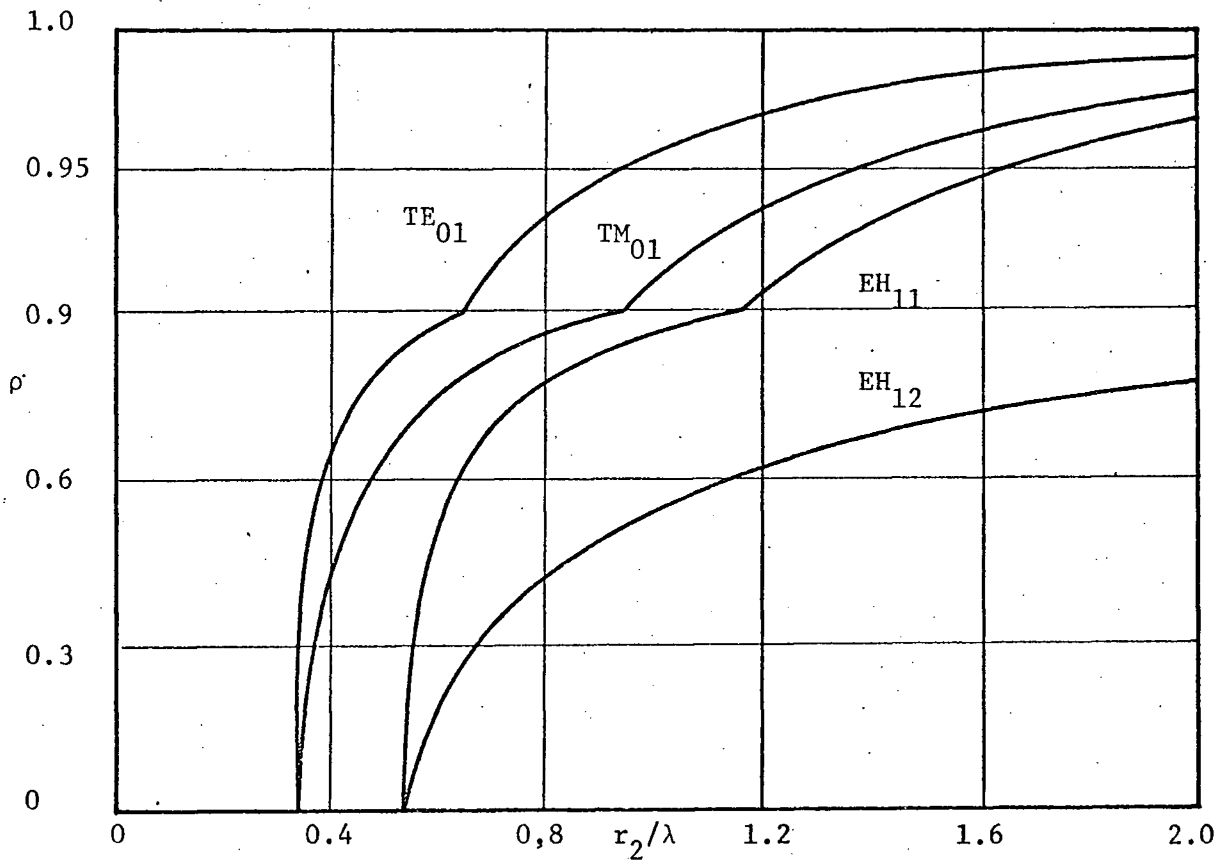

Figure 2.3 Cutoff Conditions; TE_{01}, TM_{01}, EH_{11} and HE_{12} Modes

3. CAVITY-RESONANCE METHOD FOR MEASURING ATTENUATION

3.1 Introduction

The cavity-resonance method appeared to be the one most suitable for directly measuring the small attenuation coefficient of the HE_{11} mode on dielectric-tube waveguides. The main advantages of the method are that only a fairly short length of waveguide is needed and the problems of accurate measurement of power levels or substituted attenuation are avoided. The relationship between attenuation coefficient and the Q factor of a cavity formed from a section of the waveguide and two metallic end plates is discussed in the next section.

3.2 Relation Between Attenuation Coefficient and Q Factor

Adopting the nomenclature of reference 7, the Q factor of the resonator is given by[8]

$$Q = \frac{\omega WL}{2N_p + NL} = \frac{\omega L N_g/v_g}{2N_p + 2L\alpha N_g} \quad \text{.......... 3.1}$$

where

$$W = N_g/v_g, \quad N = 2\alpha N_g$$

Then

$$\frac{1}{Q} = \frac{2\alpha v_g}{\beta v_p} + \frac{2N_p}{\omega WL} \quad \text{.......... 3.2}$$

where

$$\beta = \omega/v_p = 2\pi/\lambda_g$$

For very long resonators, the second term in equation 3.2 can be neglected and the expression for Q becomes

$$Q \simeq \frac{\beta}{2\alpha}\left(\frac{v_p}{v_g}\right) \quad \text{.......... 3.3}$$

Then the attenuation coefficient α is given by

$$\alpha \simeq \frac{\beta}{2Q}\left(\frac{v_p}{v_g}\right) \qquad 3.4$$

In previous experimental investigations of surface waveguides[4,9], values of α have been obtained by measuring Q and β and using the transmission-line formula,

$$\alpha = \frac{\beta}{2Q} \qquad 3.5$$

which assumes $v_p/v_g=1$ in equation 3.4. This assumption may lead to significant errors. As an example, the factor v_p/v_g for the dominant HE_{11} mode on a polythene tube ($\varepsilon_{r2}=2.26$) waveguide has been completed and is shown in figure 3.1. Inspection of this figure shows that equation 3.5 is valid for such waveguides when the phase-velocity reduction is very small or very large, but can lead to appreciable errors for intermediate values.

In the present investigation, no provision was made for measuring v_g and hence the ratio v_p/v_g together with the term in equation 3.2 involving end plate losses were evaluated using the theory given below.

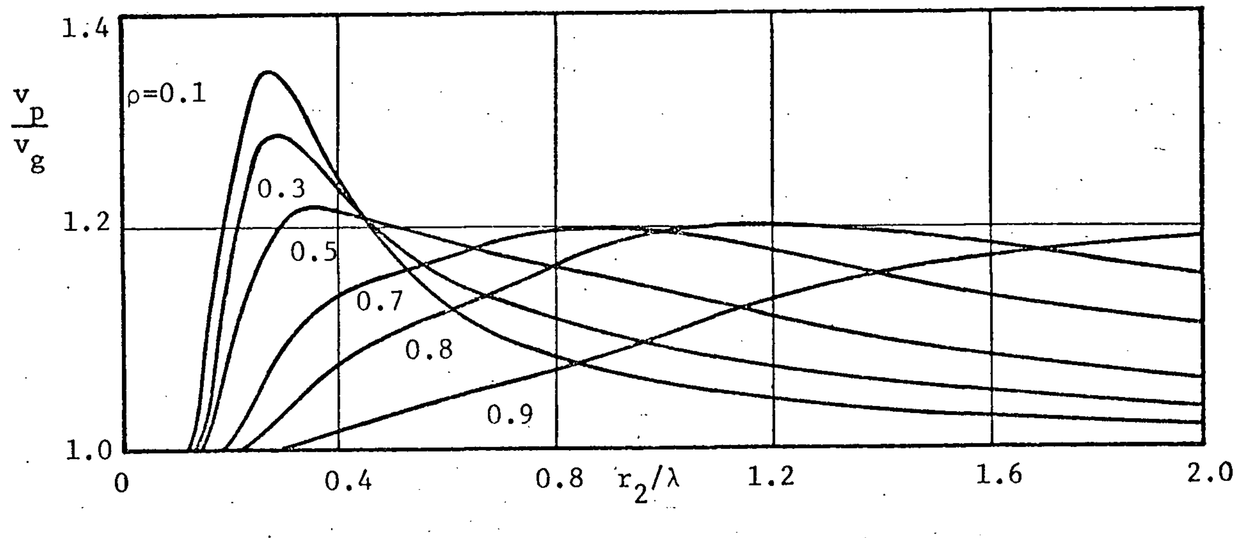

Figure 3.1 Characteristics of Dielectric-Tube Waveguide, HE_{11} Mode

3.2.1 Relation Between Attenuation Coefficient and Q Factor for Surface-Wave Resonator

From equation 3.2,

$$\alpha = \frac{\beta}{2}\left(\frac{v_p}{v_g}\right)\left(\frac{1}{Q} - \frac{2Np}{\omega WL}\right) = \frac{\beta}{2}\left(\frac{v_p}{v_g}\right)\left(\frac{1}{Q} - \frac{2(N_{p1}+N_{p2}+N_{p3})}{\omega L(W_1+W_2+W_3)}\right) \qquad \ldots 3.6$$

where, for the dominant HE_{11} mode,

$$\left.\begin{aligned}
W_1 &= \frac{a_2 a_2^* \pi\varepsilon_{r1}}{4v_0 Z_0 h_1^4}\left(\frac{A_1^2(p_{21})}{I_1^2(p_{11})}\right)\left[h_1^2\, T_I + \left[\beta^2+(k_0 Z_0 c_1)^2\right] S_I - 4\beta k_0 Z_0 c_1 I_1^2(p_{11})\right] \\
W_2 &= \frac{a_2 a_2^* \pi\varepsilon_{r2}}{4v_0 Z_0 h_2^4}\left[h_2^2\, T_A + \beta^2 S_A + (k_0 Z_0 c_2)^2 S_B + 4\beta k_0 Z_0 c_2 S_{AB}\right] \\
W_3 &= \frac{a_2 a_2^* \pi\varepsilon_{r3}}{4v_0 Z_0 h_3^4}\left(\frac{A_1^2(p_{22})}{K_1^2(p_{32})}\right)\left[h_3^2\, T_k + \left[\beta^2+(k_0 Z_0 c_3)^2\right] S_K + 4\beta k_0 Z_0 c_3 K_1^2(p_{32})\right]
\end{aligned}\right\} \ldots 3.7$$

$$\left.\begin{aligned}
N_{p1} &= \frac{2a_2 a_2^* \pi R_m}{h_1^4}\left(\frac{A_1^2(p_{21})}{I_1^2(p_{11})}\right)\left[\left(\frac{k_0\varepsilon_{r1}}{Z_0}\right)^2 \cdot S_I + c_1^2\beta^2 S_I - 4c_1\beta\left(\frac{k_0\varepsilon_{r1}}{Z_0}\right)\cdot I_1^2(p_{11})\right] \\
N_{p2} &= \frac{2a_2 a_2^* \pi R_m}{h_2^4}\left[\left(\frac{k_0\varepsilon_{r2}}{Z_0}\right)^2 \cdot S_A + c_2^2\,\beta^2\left(\frac{A_1^2(p_{21})}{B_1^2(p_{21})}\right) S_B + 4c_2\beta\left(\frac{k_0\varepsilon_{r2}}{Z_0}\right)\left(\frac{A_1(p_{21})}{B_1(p_{21})}\right) S_{AB}\right] \\
N_{p3} &= \frac{2a_2 a_2^* \pi R_m}{h_3^4}\left(\frac{A_1^2(p_{22})}{K_1^2(p_{32})}\right)\left[\left(\frac{k_0\varepsilon_{r3}}{Z_0}\right)^2 \cdot S_K + c_3^2\beta^2 S_K + 4c_3\beta\left(\frac{k_0\varepsilon_{r3}}{Z_0}\right) K_1^2(p_{32})\right]
\end{aligned}\right\} \ldots 3.8$$

The functions S_I, S_A, S_B, S_{AB}, S_K, T_I, T_A and T_K are integrals of functions of Bessel functions which are defined and evaluated in reference 7. Table 3.1 shows a sample output from a computer program called QFACTOR which was used to obtain the unloaded Q factor of the surface wave resonator, the factor (v_p/v_g) and the attenuation coefficient of the dominant HE_{11} mode by solving equation 2.4.b for $k_0(\beta)$, where the phase coefficient β was decided by the number of half wavelengths contained in the length of the cavity.

R1=0.012700(M) R2=0.015875(M) R1/R2=0.8000 ER1=1.000 ER2=2.260 ER3=1.000

T1=0.0 T2=0.0005 T3=0.0 SIGMA=0.3536E 08(MHO/M) LENGTH OF THE RESONATOR=1.757(M)

L	F(HZ)	R2/LAMBDA	KO/BETA	VP/VG	QU	ALPHA(DB/M)	ALPHA(DB/FT)
95	7.8842E 09	4.1748E-01	9.7252E-01	1.0854E 00	1.0081E 04	7.8611E-02	2.3961E-02
96	7.9606E 09	4.2153E-01	9.7171E-01	1.0865E 00	9.8862E 03	8.1105E-02	2.4721E-02
97	8.0368E 09	4.2557E-01	9.7091E-01	1.0875E 00	9.7002E 03	8.3622E-02	2.5488E-02
98	8.1130E 09	4.2960E-01	9.7010E-01	1.0885E 00	9.5222E 03	8.6165E-02	2.6263E-02
99	8.1889E 09	4.3362E-01	9.6930E-01	1.0895E 00	9.3519E 03	8.8731E-02	2.7045E-02
100	8.2648E 09	4.3764E-01	9.6849E-01	1.0905E 00	9.1886E 03	9.1321E-02	2.7835E-02
101	8.3405E 09	4.4165E-01	9.6769E-01	1.0915E 00	9.0322E 03	9.3934E-02	2.8631E-02
102	8.4161E 09	4.4565E-01	9.6689E-01	1.0924E 00	8.8818E 03	9.6573E-02	2.9436E-02
103	8.4916E 09	4.4965E-01	9.6609E-01	1.0933E 00	8.7372E 03	9.9236E-02	3.0247E-02
104	8.5669E 09	4.5364E-01	9.6529E-01	1.0942E 00	8.5980E 03	1.0192E-01	3.1067E-02
105	8.6421E 09	4.5762E-01	9.6449E-01	1.0951E 00	8.4641E 03	1.0463E-01	3.1893E-02
106	8.7172E 09	4.6160E-01	9.6369E-01	1.0960E 00	8.3349E 03	1.0737E-01	3.2727E-02
107	8.7922E 09	4.6557E-01	9.6289E-01	1.0968E 00	8.2103E 03	1.1013E-01	3.3569E-02
108	8.8671E 09	4.6953E-01	9.6210E-01	1.0977E 00	8.0898E 03	1.1292E-01	3.4419E-02
109	8.9418E 09	4.7349E-01	9.6131E-01	1.0985E 00	7.9735E 03	1.1574E-01	3.5277E-02
110	9.0164E 09	4.7744E-01	9.6052E-01	1.0993E 00	7.8611E 03	1.1857E-01	3.6142E-02
111	9.0909E 09	4.8138E-01	9.5973E-01	1.1001E 00	7.7521E 03	1.2144E-01	3.7016E-02
112	9.1653E 09	4.8532E-01	9.5895E-01	1.1009E 00	7.6466E 03	1.2433E-01	3.7897E-02
113	9.2396E 09	4.8926E-01	9.5816E-01	1.1017E 00	7.5443E 03	1.2725E-01	3.8787E-02
114	9.3138E 09	4.9318E-01	9.5738E-01	1.1025E 00	7.4451E 03	1.3020E-01	3.9685E-02
115	9.3878E 09	4.9710E-01	9.5660E-01	1.1033E 00	7.3489E 03	1.3317E-01	4.0591E-02
116	9.4617E 09	5.0102E-01	9.5582E-01	1.1041E 00	7.2553E 03	1.3617E-01	4.1506E-02
117	9.5356E 09	5.0493E-01	9.5505E-01	1.1048E 00	7.1645E 03	1.3920E-01	4.2429E-02
118	9.6093E 09	5.0883E-01	9.5427E-01	1.1056E 00	7.0761E 03	1.4226E-01	4.3360E-02
119	9.6829E 09	5.1273E-01	9.5350E-01	1.1063E 00	6.9902E 03	1.4534E-01	4.4301E-02
120	9.7564E 09	5.1662E-01	9.5273E-01	1.1071E 00	6.9065E 03	1.4846E-01	4.5250E-02

Table 3.1 Sample Output from QFACTOR

3.3 Relation Between Unloaded Q and Loaded Q

In practice the loaded Q factor, Q_ℓ, of a cavity resonator is given by

$$Q_\ell = \frac{f_r}{\Delta f} \quad \text{.....................3.9}$$

where f_r is the resonant frequency and Δf is the bandwidth at the half-power points of the transmission characteristic.

To determine the bandwidth Δf, either the amplitude or the phase of the transmission characteristic of the resonator can be used (figure 3.2[10]).

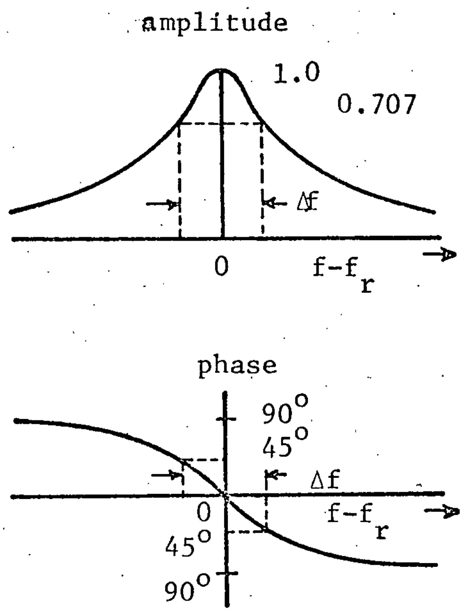

Figure 3.2 Transmission Characteristics of a Resonant Cavity

The unloaded Q can be obtained by measuring the loaded Q and the coupling coefficients of the cavity input and output apertures. In the case where there are two coupling apertures, the unloaded Q is given by

$$Q_u = Q_\ell(1+\beta_1+\beta_2) \quad \text{...........3.10}$$

In the case where the output coupling β_2 is negligibly small, equation 3.10 becomes

$$Q_u \simeq Q_\ell(1+\beta_1) \quad \text{.............3.11}$$

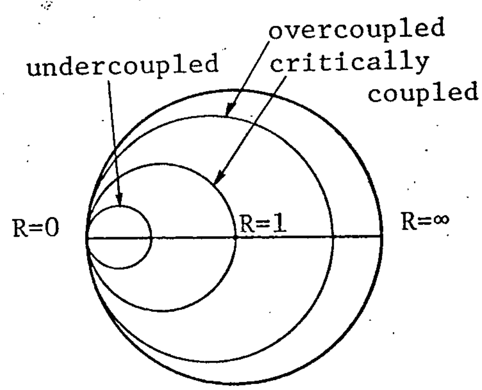

Figure 3.3 Variation of Input Impedance of a Resonant Cavity

To obtain the coupling coefficient β_1, it is necessary to measure the input impedance of the resonator at resonance. If the normalized resistive component R, which is equal to the coupling coefficient β_1 is found to be greater than unity, the cavity is overcoupled. If R is found to be less than unity, the cavity is undercoupled and if R is found to be unity the cavity is critically coupled.

4. EXPERIMENTAL APPARATUS

4.1 Introduction

Although dielectric-tube waveguides would be most advantageously used at millimeter-wave frequencies, it was more convenient to conduct the present investigation at X-band frequencies. This placed less stringent tolerance requirements on the dimensions of the tube, making it possible to use commercially available tubes.

The general layout of the microwave apparatus is shown in figure 4.1.

To improve the frequency stability of the X-13 klystron, the latter was water cooled and a klystron synchronizer (FEL Model 136-AF) was used. For measurement of the Q factor of the surface-wave resonator, it was necessary to measure the bandwidth Δf of the resonator Q curve accurately. This was facilitated by use of a beat-frequency technique which made it possible to measure frequencies in the X-band range with an error of not more than ± 50 KHz. By comparison, the ordinary reaction type of cavity frequency meter has a typical accuracy of ± 1MHz in the same frequency range.

Details of the components of the surface-wave resonator are given in the following sections.

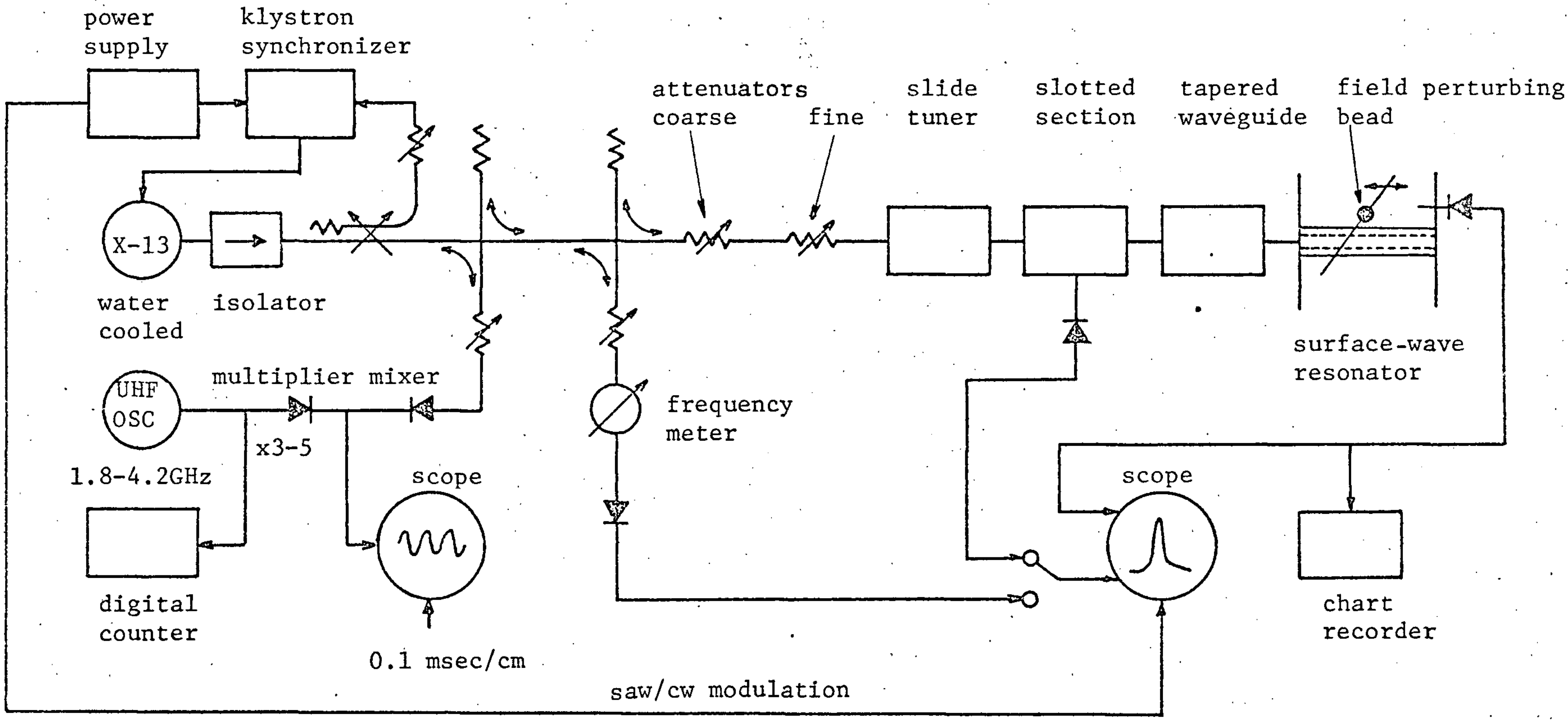

Figure 4.1 Layout of Apparatus

4.2 Surface-Wave Resonator

The surface-wave resonator, shown in figures 4.2-4.5, consisted of a length of dielectric tube [1]* approximately 1.78m long bounded at both ends by flat, circular, aluminum plates, 0.61m in diameter and 1.2 cm in thickness, mounted at right angles to the waveguide. Since it was desirable to use as long and as straight a tube as possible in order to obtain accurate measurements of the attenuation coefficient, it was necessary to devise some method of adequately supporting and tensioning the tube. This was achieved by passing the ends through holes in the end plates of the resonator and radially gripping the tube walls between these plates and close fitting, circular, short-circuiting plugs, [2 and 3], inside the tube. Leakage of energy outside the resonator through the dielectric-filled, annular apertures thus formed in the end plates was prevented by the use of annular short-circuiting plungers [4] at each end of the dielectric tube. The end plates of the resonator were kept parallel and in alignment by four tie rods [5]. Alignment of the end plates was carried out using a laser in a manner similar to that used for aligning optical cavities. Table 4.1 shows details of the polythene tubes used in the investigation.

The other end plate of the resonator had a number of holes [7], 0.13 cm in diameter, lying along a radius of the plate, through which was inserted a small wire probe sensitive to the longitudinal component of the electric field within the resonator. By moving the probe from one sampling hole to another the radial field decay could be investigated. Normally, all the holes in the end plate, except the one containing the probe, were closed by tightly fitting aluminum plugs.

---

* The numbers given in the text correspond to those appearing in figures 4.3-5.

For the measurement of the radial decay of the radial component of the electric field inside the resonator, another probe, mounted on a modified slotted-line carriage, was moved radially across some cross-sectional plane inside the resonator.

tube	r_1(cm)	r_2(cm)	$\rho=r_1/r_2$
I	0.953	1.270	0.750
II	1.270	1.588	0.800
III	1.588	1.905	0.833

Table 4.1 Details of Polythene Tubes

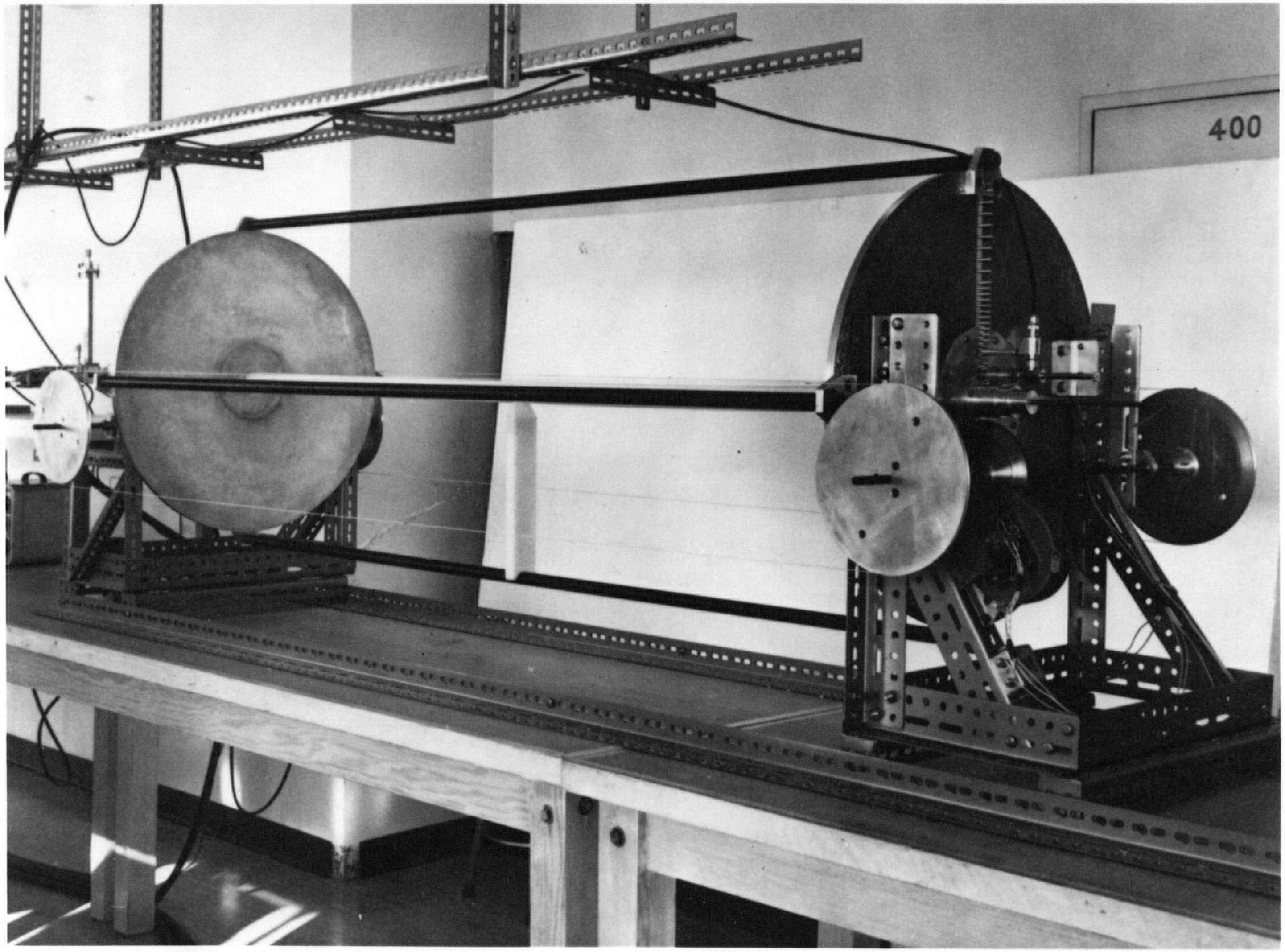

Figure 4.2 General View of Surface-Wave Resonator

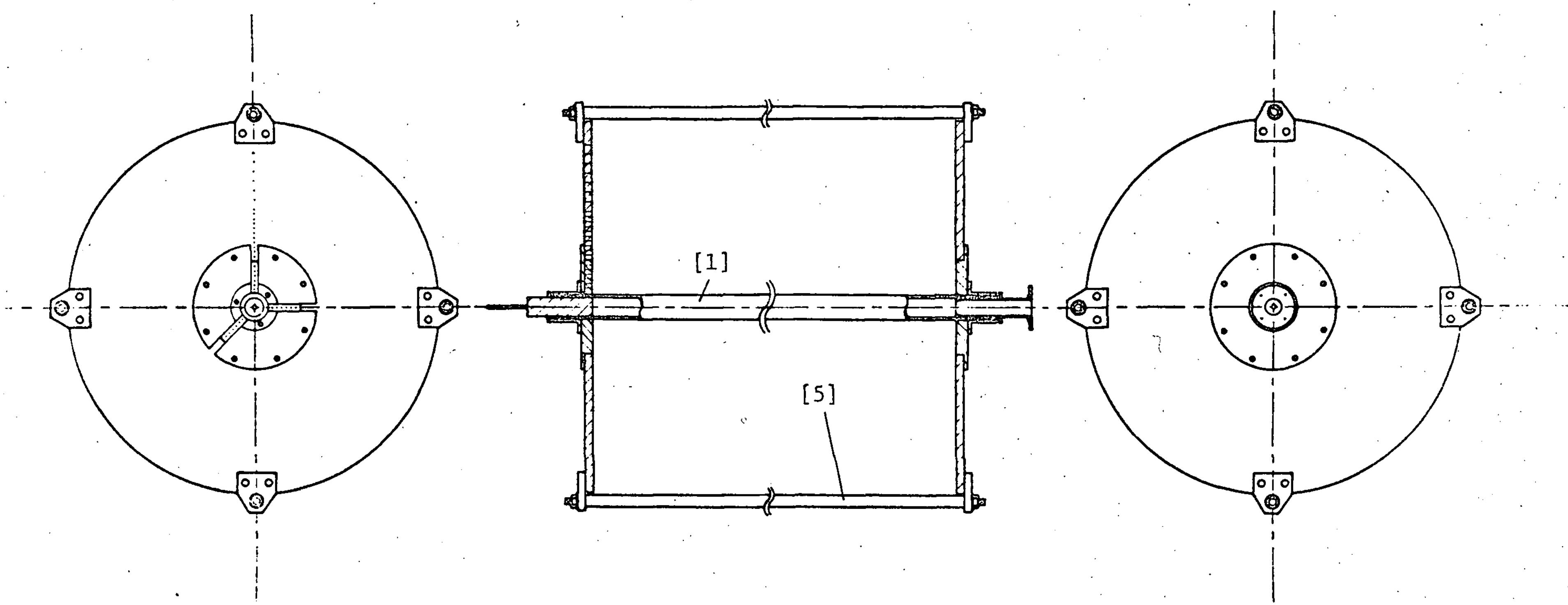

Figure 4.3 Surface-Wave Resonator

scale 1/10

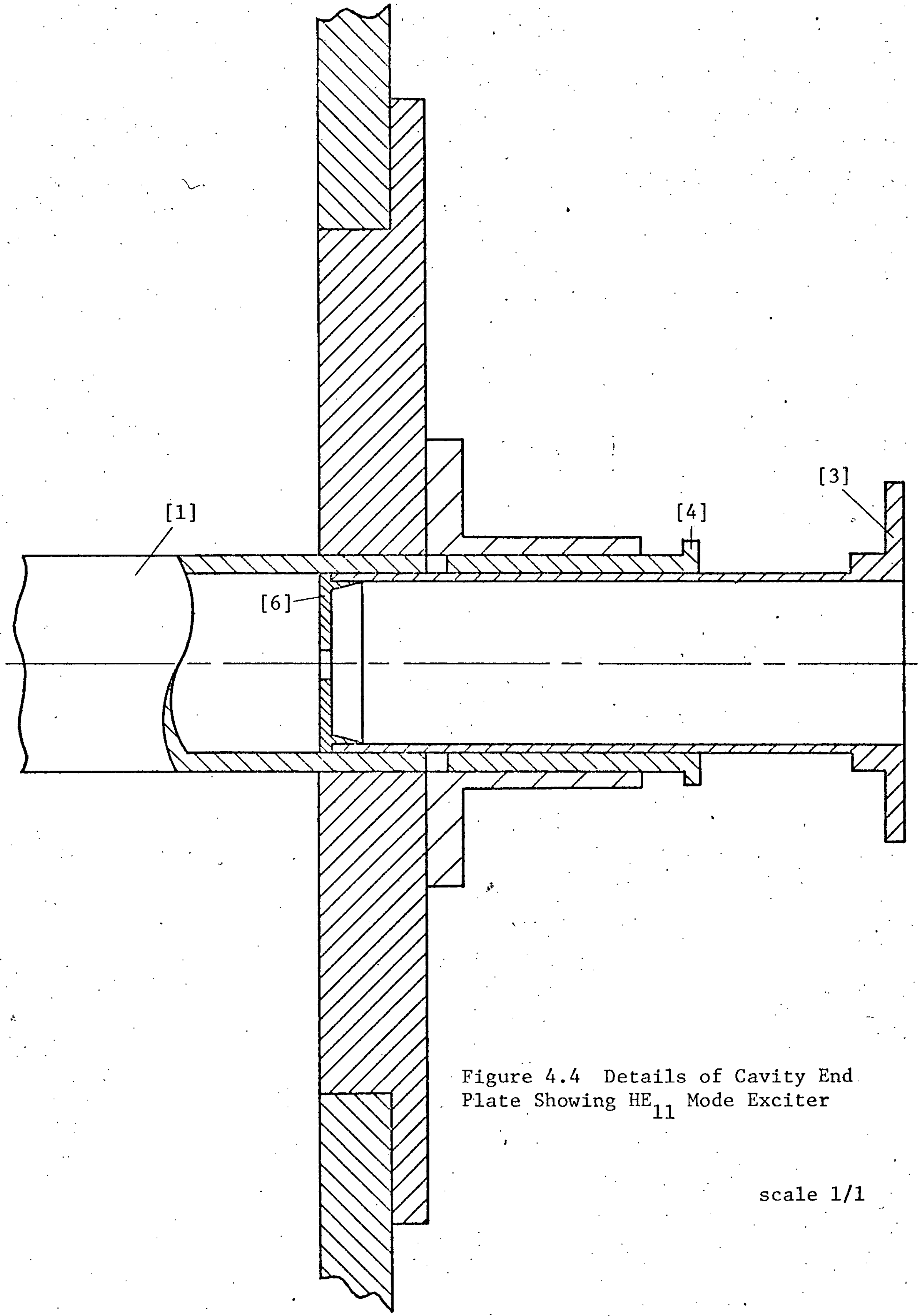

Figure 4.4 Details of Cavity End Plate Showing HE_{11} Mode Exciter

scale 1/1

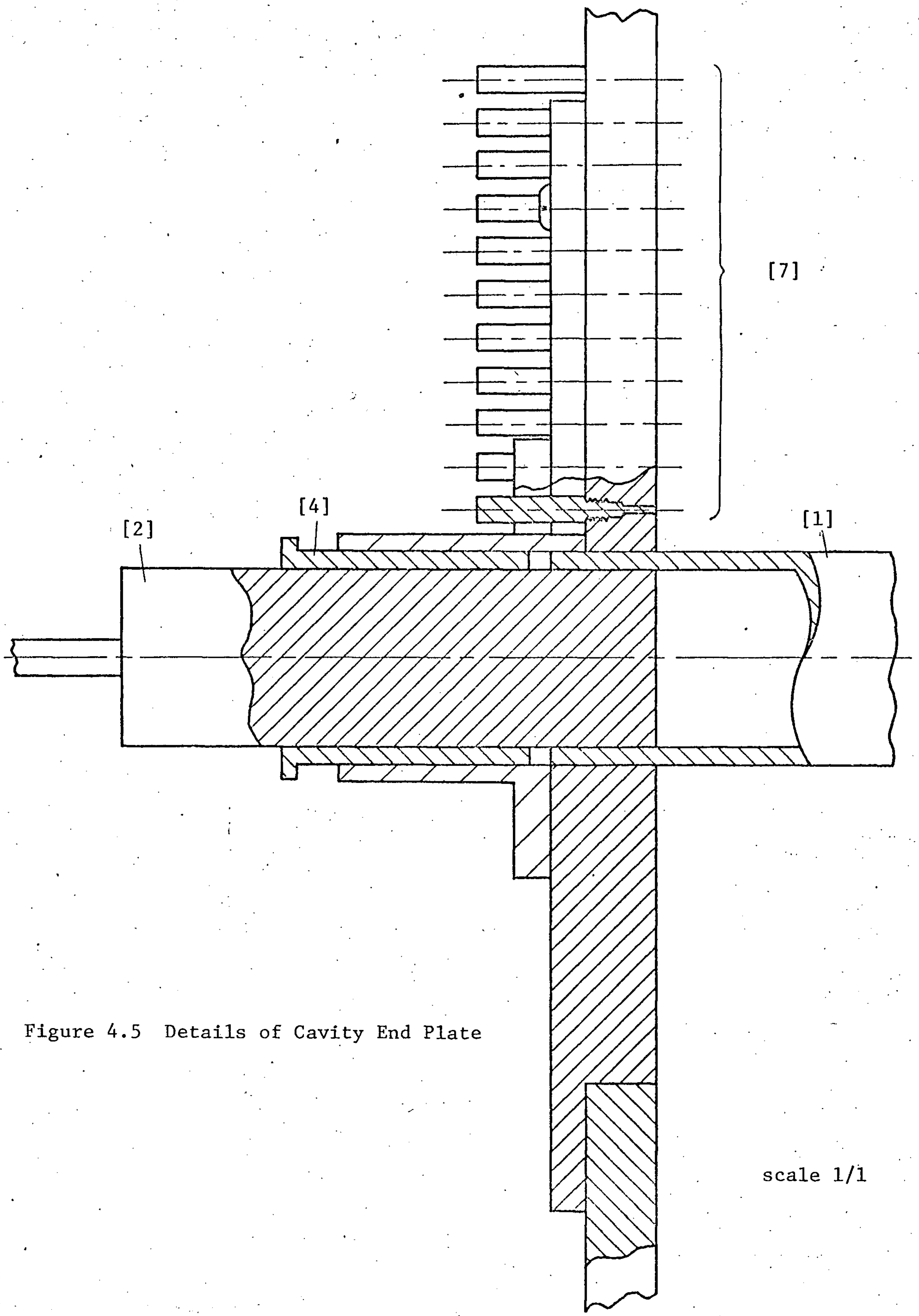

Figure 4.5 Details of Cavity End Plate

scale 1/1

4.3 Mode Exciters

Excitation of the dominant HE_{11} mode on the dielectric tube was achieved by means of a small circular aperture [6] fed by a circular waveguide, which also formed one of the tube tensioning plugs [3] mentioned in section 4.2.

Excitation of the TE_{01} mode was achieved by replacing the annular short-circuiting plunger [4] at the input end of the resonator by two polystyrene-filled rectangular waveguides of transverse dimensions 0.8 cm by 1.3 cm (figure 4.7), which butted up against the exposed end of polythene tube III. The waveguides were excited 180^{o} (figure 4.6.b) out of phase by using the set-up shown in figure 4.6.a. The dimensions of the tapered wave-quides were such as to equalize the phase velocities of the $TE^{\square}_{10}$ mode of the exciter and the TE^{o}_{01} mode of the surface waveguide. This arrangement could also be used to excite the dominant HE_{11} mode by feeding both dielectric waveguides in phase. An alternative method of exciting the TE_{01} mode, that due to

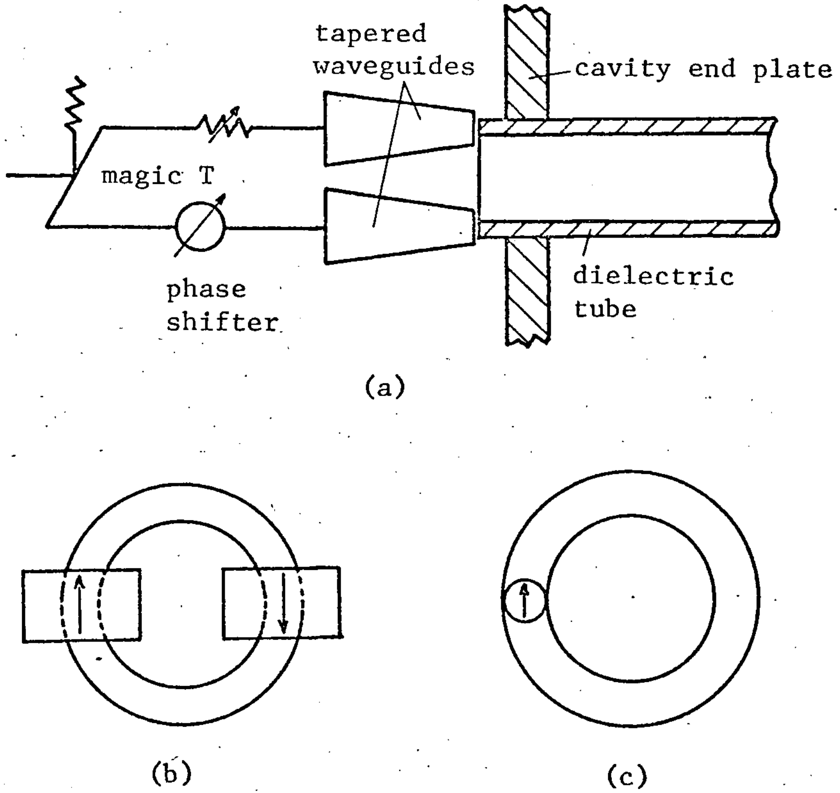

Figure 4.6 Diagram of TE_{01} Mode Exciter and the Position of Exciter Relative to Dielectric Tube

Astrahan[3], is shown in Figure 2.6.c. This was tried in the present investigation, but proved to be unsatisfactory, since it excited both the HE_{11} and TE_{01} modes simultaneously.

For excitation of the TM_{01} mode, the circular waveguide and aperture were replaced by a section of coaxial line, having a tapered inner conductor. This is shown in figure 4.8.

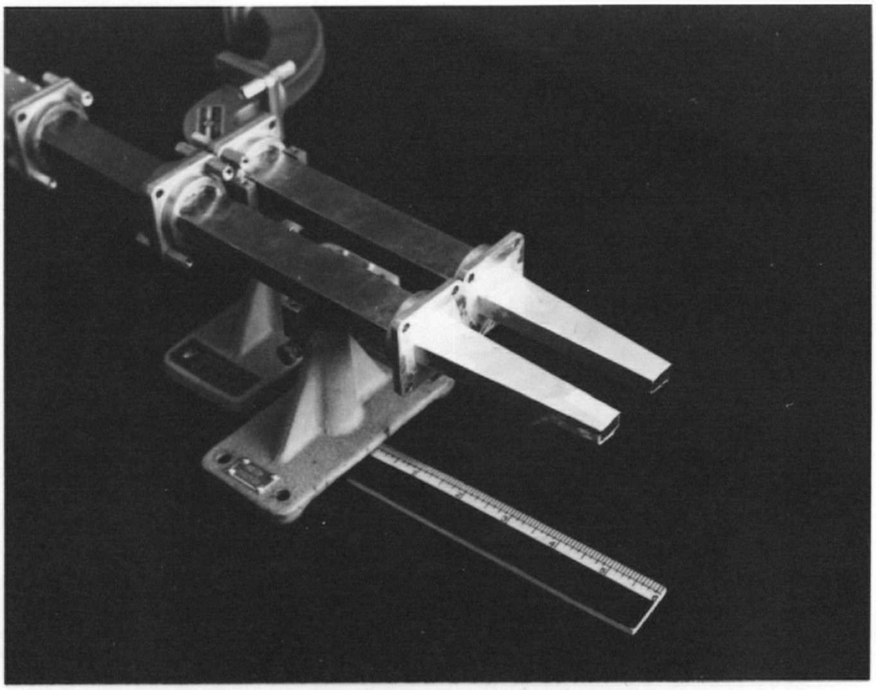

Figure 4.7 TE_{01} Mode Exciter

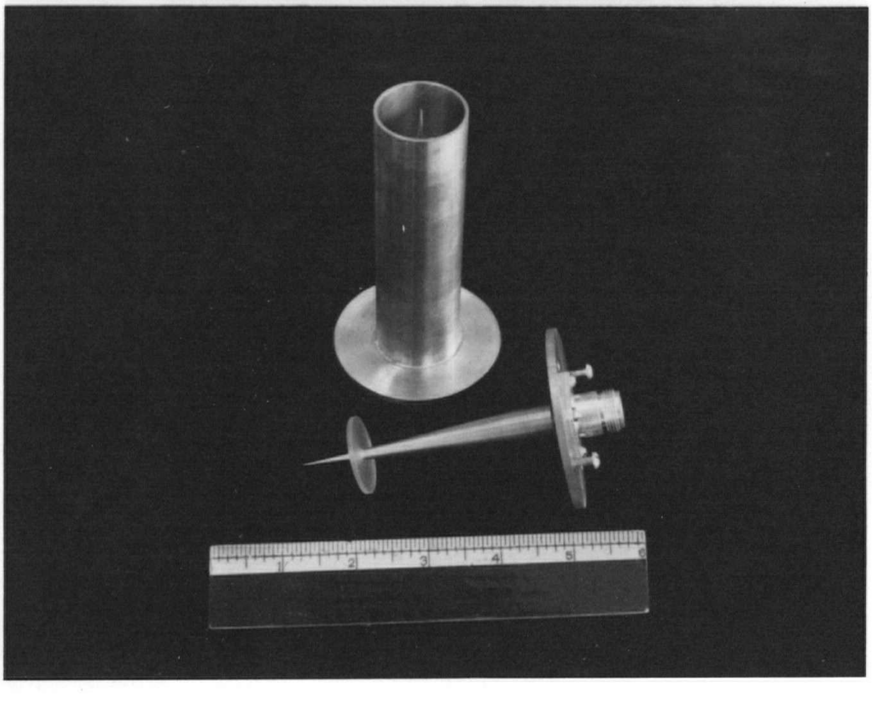

Figure 4.8 TM_{01} Mode Exciter

5. RESULTS

5.1 Dependence of Cavity Q Factor on Size of Coupling Aperture

Figure 5.1 shows the dependence of the cavity Q factor of the HE_{11} mode on coupling aperture size for tube II at a frequency of 8.328 GHz. For aperture sizes of less than about 5 mm, both the loaded Q factor and the unloaded Q factor became virtually constant and the coupling coefficient β_1 was smaller than 0.01. Hence the amount of cavity loading for this range of aperture sizes was negligible. Table 5.1 shows the actual size of aperture used with each particular size of tube. In all cases, the apertures were small enough to ensure that the errors in the measurements were small.

tube	diameter of aperture (mm)
I	7.1
II	6.4
III	6.4

Table 5.1 Details of Coupling Apertures

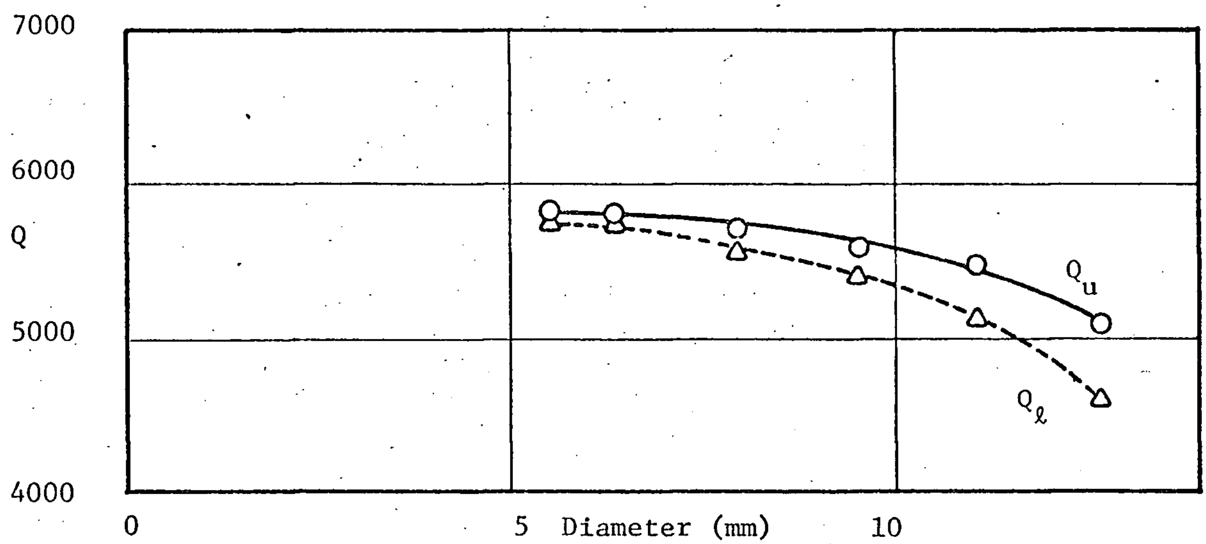

Figure 5.1 Measured Dependence of Cavity Q Factor of HE_{11} Mode on Coupling Aperture Diameter, tube II, f=8.328GHz
O experimental points for unloaded Q factor
Δ experimental points for loaded Q factor

5.2 Measurement of Guide Wavelength

Measurement of the wavelength along the surface of the dielectric-tube mounted inside the resonator was carried out using a perturbation method similar to that described by Barlow and Karbowiak[11]. Essentially the method involved the determination of the number of half wavelengths contained in the length of the resonator when the latter was resonant at a known frequency. This was achieved with the aid of a small aluminum bead supported in close proximity to the dielectric waveguide by a cotton thread stretched transversely between two parallel nylon running cords mounted longitudinally outside the resonator and diametrically opposite one another. By simultaneous axial movement of the running cords the small bead was made to traverse the length of the resonator, remaining throughout at approximately the same distance from the dielectric-waveguide. While no appreciable disturbance of the field was produced by the cotton thread, some energy was scattered by the bead except when it was situated at a node of the electric field. Thus the output of the probe connected to the resonator exhibited successive variations as the bead was moved along the dielectric waveguide, and it was only necessary to count the number of oscillations in the probe output in traversing the length of the resonator. The number of maxima corresponded to the number of nodes in the longitudinal field distribution of the resonator and the wavelength was therefore determined. Thus, the accuracy of the method was dependent on the precision with which the length of the resonator could be measured. In the present investigation, this was achieved to an accuracy better than ± 1 mm, leading to an error in the measurement of guide wavelength of not more than 1 part in 1780. Figure 5.2 shows a typical probe output, obtained when the field perturbing

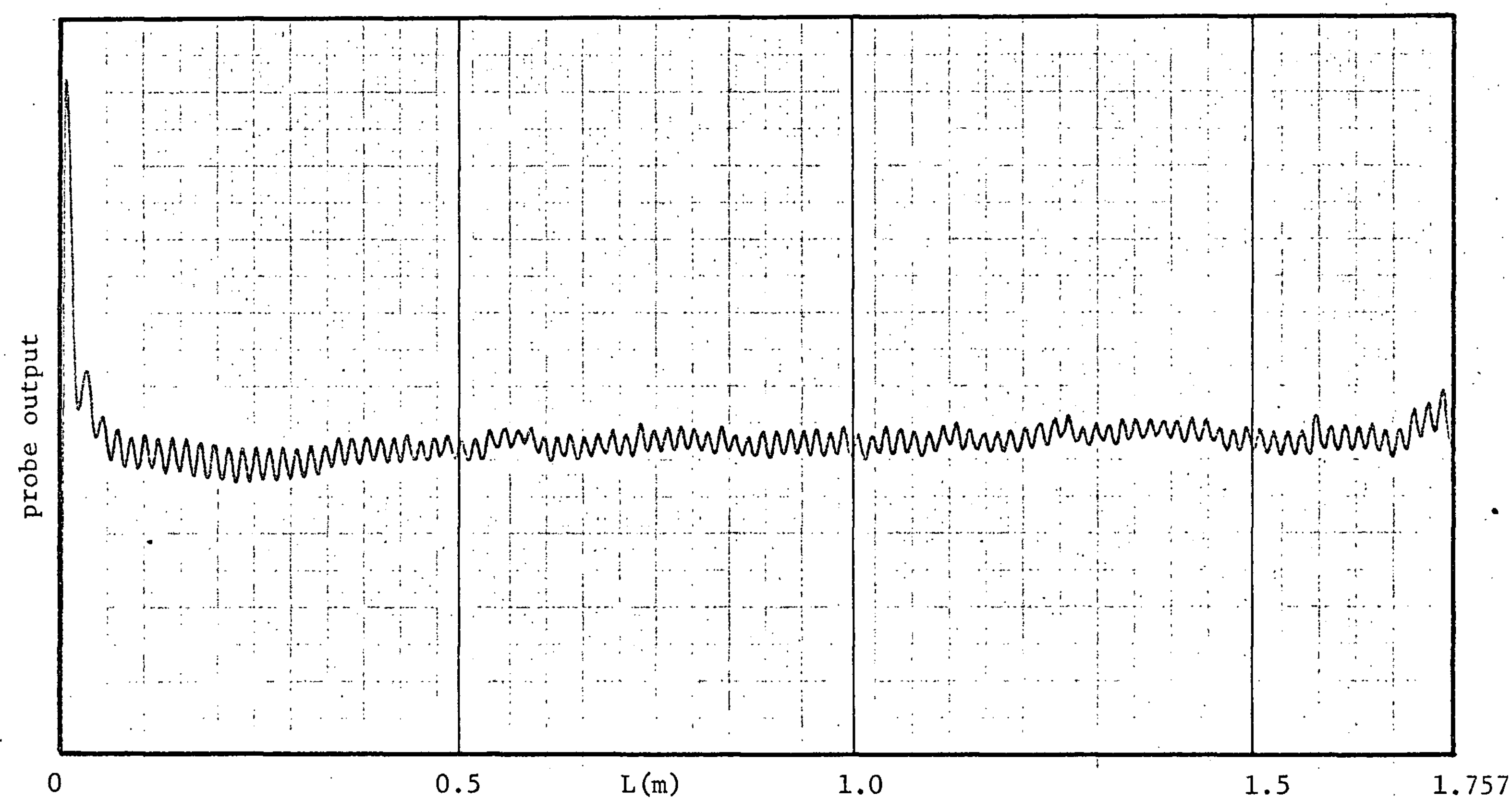

Figure 5.2 Measurement of Guide Wavelength of HE_{11} Mode by Field Perturbing Bead Method, Tube III, f=8.323 GHz, ℓ=101

bead was moved along the length of the resonator. From this, it was deduced that there were 101 half wavelengths in the length of the resonator at a frequency of 8.323 GHz.

The measured and theoretically predicted variation of the guide wavelength of the HE_{11} mode with r_2/λ is shown in figures 5.3.a-c for tubes I, II and III. The experimental results agree well with particular theoretical curves computed for values of relative permittivity in the range 2.26 to 2.31. (The exact dielectric properties of the commercially available polythene tubes used were not known.)

As a check on the cutoff frequencies of the higher order TE_{01} and TM_{01} modes, the latter were individually excited on tube III, using the appropriate mode exciter and the variation of guide wavelength with r_2/λ at frequencies close to cutoff was measured. Good agreement between experiment and theory was obtained using the particular value of relative permittivity for tube III found before, ε_r=2.26. These results are shown in figure 5.3.c.

Figure 5.3.b shows the effect of surrounding tube II by a low-density polyfoam shield of cross-sectional dimensions 50 cm by 50 cm. As can be seen, the dispersion characteristics of the shielded tube are little different from those of the unscreened tube. The experimental results agreed most closely with the theoretical ones when the relative permittivity of the polyfoam shield was assumed to be 1.041.

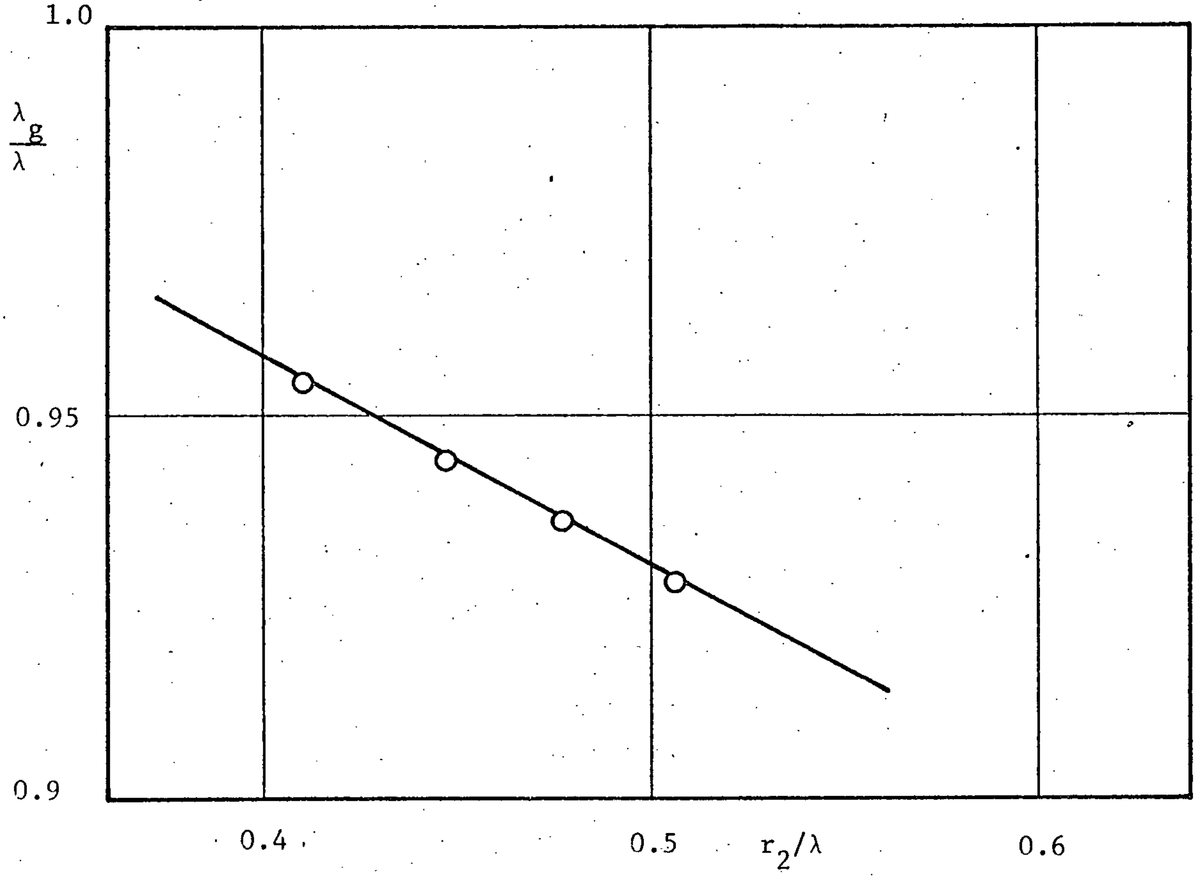

Figure 5.3.a Experimental and Theoretical Phase Characteristics of HE_{11} Mode on Polythene Tube I

O experimental points

— theoretical curve for ε_{r2}=2.31

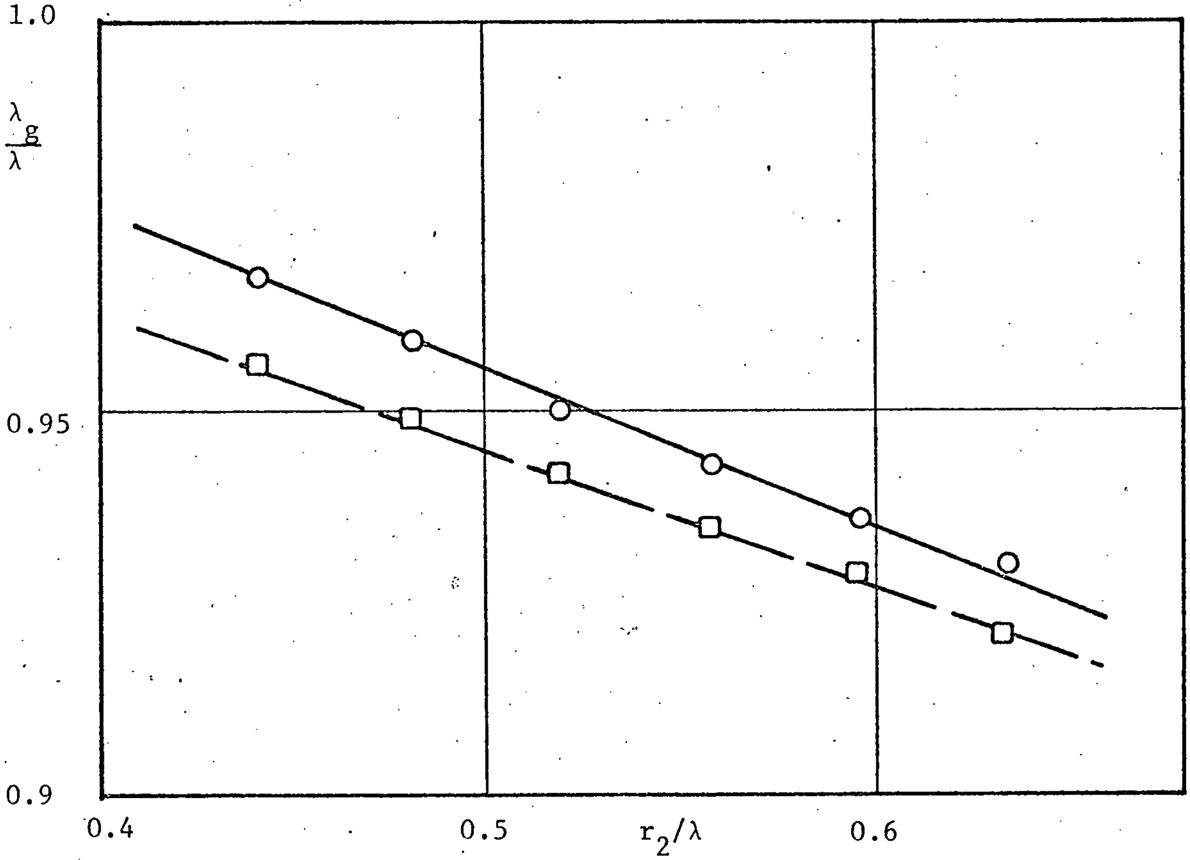

Figure 5.3.b Experimental and Theoretical Phase Characteristics of HE_{11} Mode on Shielded and Unshielded Polythene Tube II

(i) unshielded tube

○ experimental points

——— theoretical curve for $\varepsilon_{r2}=2.28$

(ii) shielded tube

□ experimental points

— — theoretical curve for $\varepsilon_{r2}=2.28$, $\varepsilon_{r3}=1.041$

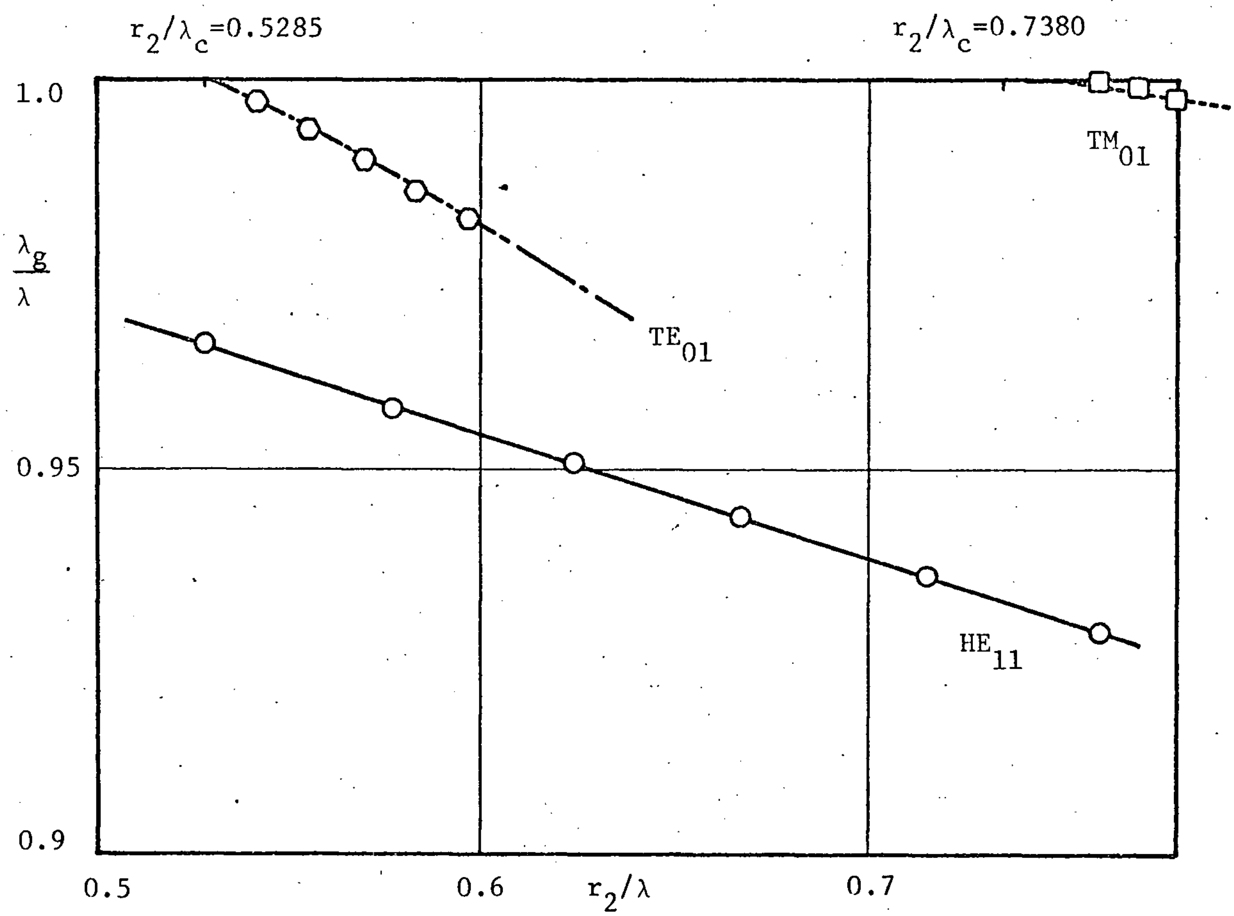

Figure 5.3.c Experimental and Theoretical Phase Characteristics of HE_{11}, TE_{01} and TM_{01} Modes on Polythene Tube III

(i) HE_{11} mode
○ experimental points
—— theoretical curve for ε_{r2}=2.26

(ii) TE_{01} mode
○ experimental points
— — theoretical curve for ε_{r2}=2.26

(iii) TM_{01} mode
□ experimental points
------ theoretical curve for ε_{r2}=2.26

5.3 Measurement of Radial Decay of Electric Field

As a check on the dispersion characteristics of the HE_{11} mode on the unscreened tube, the radial decay of the longitudinal and radial components of the electric field was measured when the resonator was resonant in the $HE_{1,1,101}$ mode at a frequency of 8.328 GHz. The results obtained for tube II are plotted in figures 5.4.a-b together with the theoretical curves computed from equations 2.2.c for ε_{r2}=2.28.

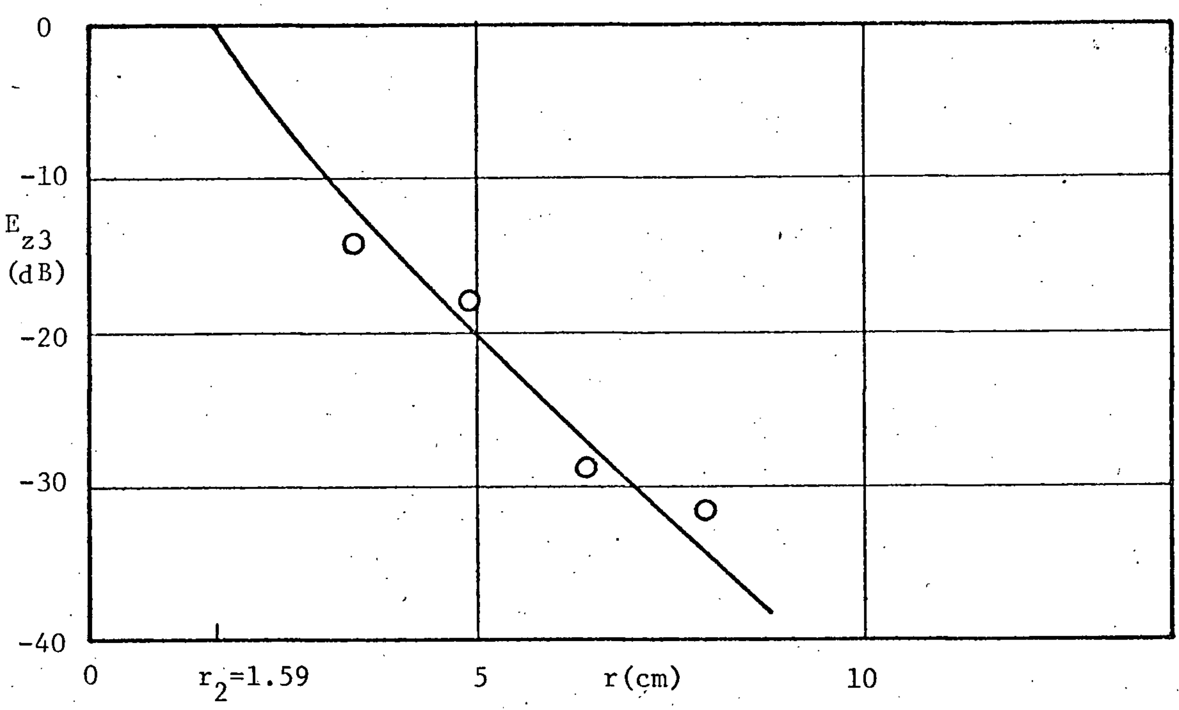

Figure 5.4.a Radial Decay of E_{z3} for HE_{11} Mode, Tube II, f=8.328GHz

O experimental points

—— theoretical curve for ε_{r2}=2.28

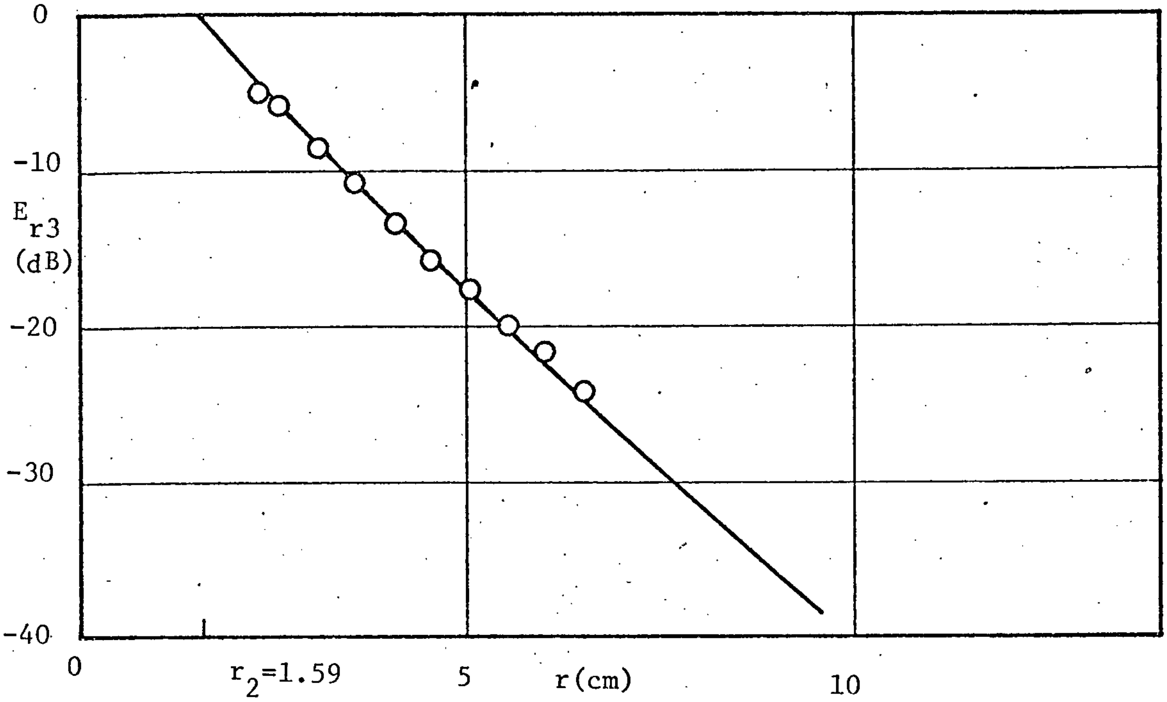

Figure 5.4.b Radial Decay of E_{r3} for HE_{11} Mode, Tube II, f=8.328 GHz
experimental points
theoretical curve for ε_{r2}=2.28

5.4 Measurement of Attenuation Coefficient

The cavity-resonance method was used to measure the relatively small attenuation coefficient of the polythene-tube waveguide. The evaluation of the attenuation coefficient from the measured Q factor of the resonator was carried out using equation 3.6.

The measured and theoretically predicted variation of the attenuation coefficient with r_2/λ of the HE_{11} mode is shown in figures 5.5.a-c for the same polythene tubes used previously. Assuming that the tubes had the values of relative permittivity found in section 5.3, it was found that the experimental points agreed with the theoretical curves for loss tangents in the range 0.00058 to 0.00085. Figure 5.5.b shows the effect of surrounding tube II by the polyfoam shield. It can be seen that the attenuation coefficient of the shielded tube is only slightly higher than that of the unshielded tube. The experimental results agree best with the theoretical ones when the loss tangent is taken to be 0.00007.

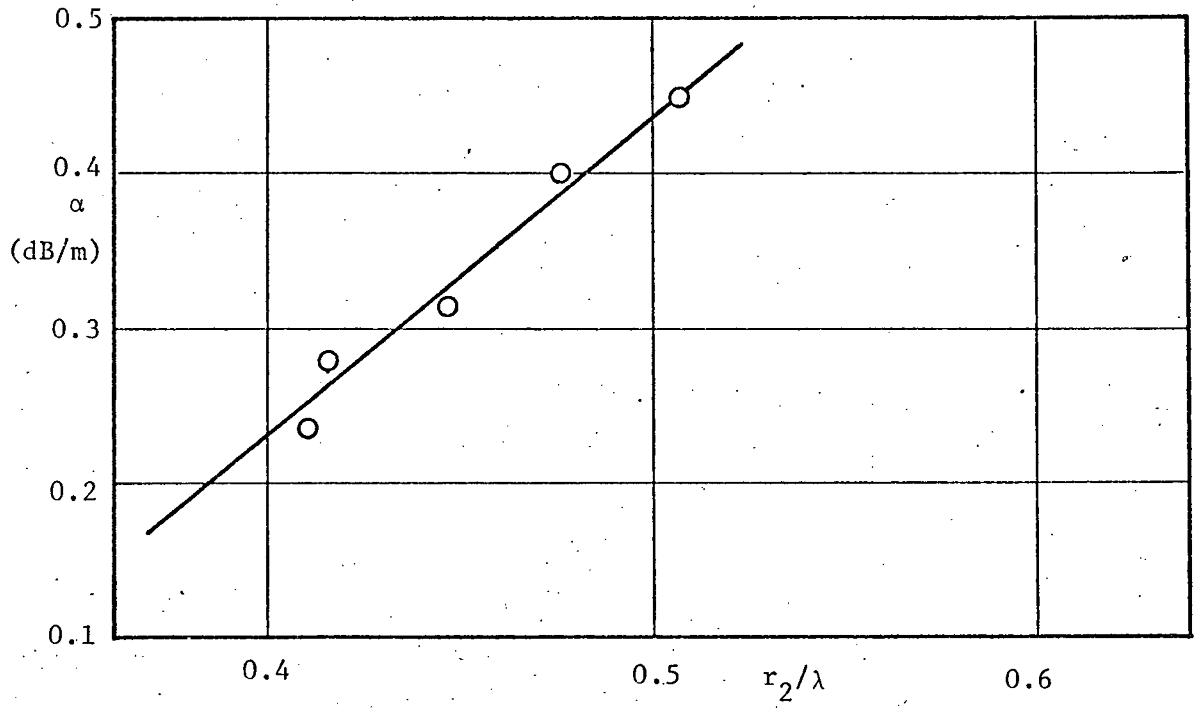

Figure 5.5.a Experimental and Theoretical Attenuation Characteristics of HE_{11} Mode on Polythene Tube I

O experimental points

— theoretical curve for ε_{r2}=2.31, $\tan\delta_2$=0.00085

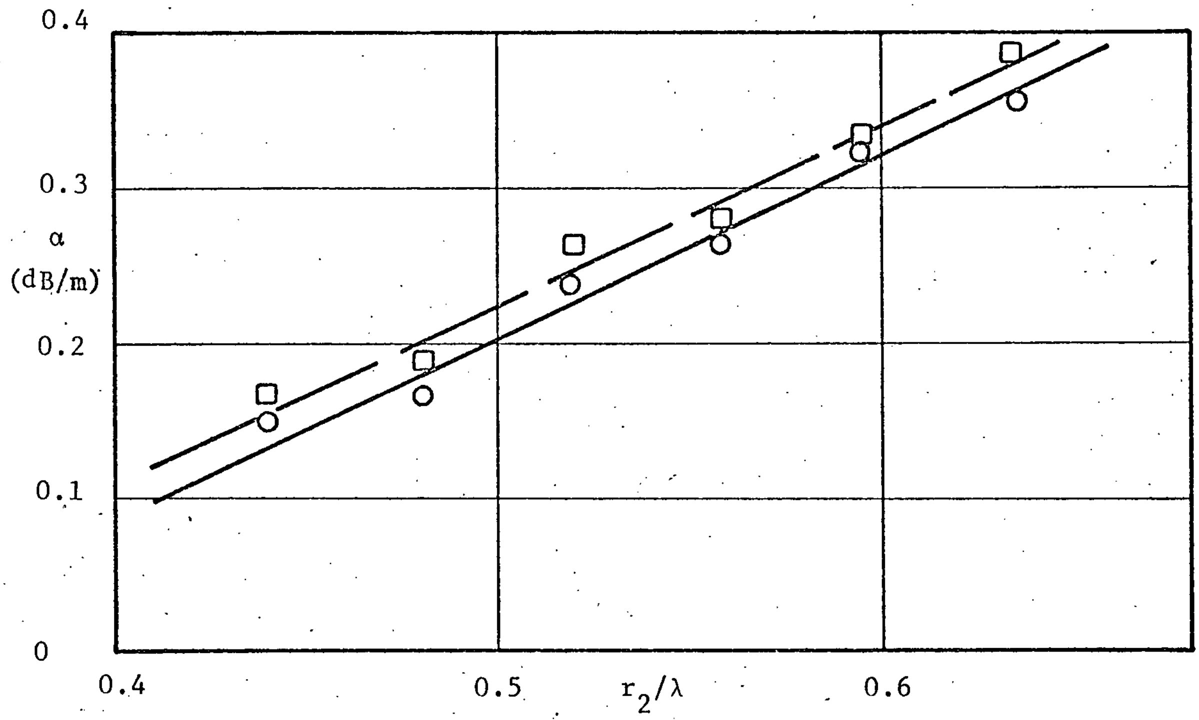

Figure 5.5.b Experimental and Theoretical Attenuation Characteristics of HE_{11} Mode on Shielded and Unshielded Polythene Tube II

(i) unshielded tube

○ experimental points

——— theoretical curve for $\varepsilon_{r2}=2.28$, $\tan\delta_2=0.00068$

(ii) shielded tube

□ experimental points

— — theoretical curve for $\varepsilon_{r2}=2.28$, $\varepsilon_{r3}=1.041$, $\tan\delta_3=0.00007$

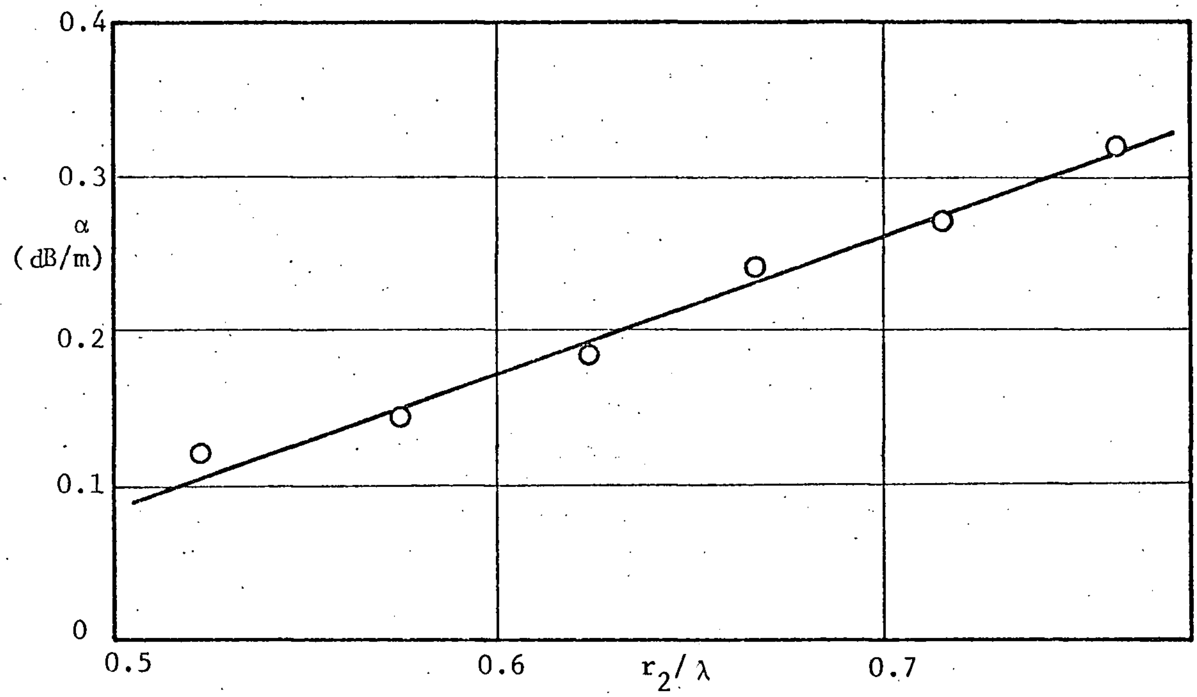

Figure 5.5.c Experimental and Theoretical Attenuation Characteristics of HE_{11} Mode on Polythene Tube III

O experimental points

—— theoretical curve for $\varepsilon_{r2}=2.26$, $\tan\delta_2=0.00058$

6. CONCLUSIONS

Accurate measurements of the attenuation coefficient of the HE_{11} mode on certain dielectric-tube waveguides have been made using a cavity-resonance method. The results obtained confirm previous theoretical predictions although there is an element of uncertainty concerning the exact dielectric properties of the commercial grade polythene tubes used. The measurements also yielded the phase coefficient of the HE_{11} mode which was confirmed by measurement of radial decay of the electric field outside the tube. Enclosing the dielectric tube in a low-density, low-loss polyfoam shield resulted in only a slight degradation of the attenuation characteristics of the waveguide.

Areas in which future theoretical and experimental work on dielectric tube waveguides might be carried out include the following:

(i) Effects of discontinuities and bends on the propagation characteristics of the HE_{11} mode

(ii) Measurement of v_g of the HE_{11} mode

(iii) Coupling between waveguides

(iv) Development of efficient mode exciters and filters

(v) Extension of all these topics to millimeter-wave frequencies

REFERENCES

1. Zachoval, L., "Elektromagnetische Wellen an dielektrischen Rohren", Ceska Akademic Ved a Umeni Praze Bulletin International, 1932, Vol. 33, P. 136.

2. Liska, J., "Elektromagneticke Vlyn na dielektricych Trubicich", Casopis pro Pestovani Maternatiky a Fysiky, 1934, Vol. 63, P. 97.

3. Astrahan, M.M., "Dielectric Tube Waveguides", Ph.D. Dissertation, Northwestern University, Illinois, 1949.

4. Jakes, W.C.,"Attenuation and Radiation Characteristics of Dielectric Tube Waveguides", Ph.D. Dissertation, Northwestern University, Illinois, 1949.

5. Unger, H., "Dielektrische Rohre als Wellenleiter", Archiv der Elektrischen Ubertragung, 1954, Vol. 8, P. 241.

6. Mallach, "Untersuchungen an dielektrischen Wellenleitern in Stab- und Rohrform", Fernmeldetech Z., 1955, Vol. 8, No. 1, P. 8.

7. Kharadly, M.M.Z., and Lewis, J.E., "Properties of Dielectric-Tube Waveguides", Proc. IEE, 1969, Vol. 116, No. 2, P. 214-224.

8. Bourk, T.R., Kharadly, M.M.Z., and Lewis, J.E., "Measurement of Waveguide Attenuation by Resonance Methods", Electronics Letters, 1968, Vol. 4, No. 13, P. 267-8.

9. Schiebe, E.H., King, B.G., Van Zeeland, D.L., "Loss Measurement of Surface Wave Transmission Lines", Journal of Applied Physics, 1954, Vol. 25, P. 790.

10. Sucher, M., and Fox, J., "Handbook of Microwave Measurement", Vol. 3, P. 470, Polytechnic Press, 1963.

11. Barlow, H.M., and Karbowiak, A.E., "An Investigation of the Characteristics of Cylindrical Surface Waves", Proc. IEE, 1953, Vol. 100, Pt. III, P. 321.